

ZScribbleSeg: A comprehensive segmentation framework with modeling of efficient annotation and maximization of scribble supervision

Ke Zhang^{a,b,1}, Bomin Wang^{a,1}, Hangqi Zhou^a, Xiahai Zhuang^{a,*}

^aSchool of Data Science, Fudan University, Shanghai, 200433, China

^bDepartment of Electrical and Computer Engineering, Johns Hopkins University, Baltimore, USA

ARTICLE INFO

Article history:

2000 MSC: 41A05, 41A10, 65D05, 65D17

Keywords: Medical Image Segmentation, Scribble Supervision, Mixture Model, Medical Image Analysis,

ABSTRACT

Curating fully annotated datasets for medical image segmentation is labour-intensive and expertise-demanding. To alleviate this problem, prior studies have explored scribble annotations for weakly supervised segmentation. Existing solutions mainly compute losses on annotated areas and generate pseudo labels by propagating annotations to adjacent regions. However, these methods often suffer from inaccurate and unrealistic segmentations due to insufficient supervision and incomplete shape information. In contrast, we first investigate the principle of good scribble annotations, which leads to efficient scribble forms via supervision maximization and randomness simulation. We further introduce regularization terms to encode the spatial relationship and the shape constraints, where the EM algorithm is utilized to estimate the mixture ratios of label classes. These ratios are critical in identifying the unlabeled pixels for each class and correcting erroneous predictions, thus the accurate estimation lays the foundation for the incorporation of spatial prior. Finally, we integrate the efficient scribble supervision with the prior into a framework, referred to as ZScribbleSeg, and apply it to multiple scenarios. Leveraging only scribble annotations, ZScribbleSeg achieves competitive performance on six segmentation tasks including ACDC, MSCMRseg, BTCV, MyoPS, Decathlon-BrainTumor and Decathlon-Prostate. Our code will be released via <https://github.com/DLwbm123/ZScribbleSeg>.

© 2026 Elsevier B. V. All rights reserved.

1. Introduction

In recent years, deep neural networks has demonstrated its potential on various visual tasks (Zhao et al., 2024). However, the success of these methods relies on massive annotations, which require labor-intensive manual efforts. For medical imaging, the dense manual labeling can take several hours to annotate just one image for experienced doctors, which is both expensive and expertise-demanding (Zhuang, 2019a). Numerous

efforts have contributed to the area of training segmentation networks with weaker annotations, including scribbles (Han et al., 2024), bounding boxes (Wei et al., 2023), points (Lin et al., 2023), and image-level labels (Kuang et al., 2023). Numerous studies have been reported utilizing only image-level labels (Kuang et al., 2023; Zhang et al., 2021; Wang et al., 2022). These methods mainly rely on large-scale training datasets, and tend to underperform on small medical image datasets. On the contrary, scribbles are suitable for labeling nested structures and easy to obtain in practice. Several works have demonstrated their potential on both semantic and medical image segmentation (Han et al., 2024; Liu et al., 2022; Khoreva et al., 2017). Therefore, we aim to investigate this specific form of weakly

*Xiahai Zhuang is the corresponding author. Email: zxh@fudan.edu.cn; Ke Zhang currently is a PhD student at Johns Hopkins University, and this work was done when she was in Fudan University.

¹These authors contributed equally to this work.

supervised medical image segmentation using only scribble annotations for model training.

Conventionally, scribble annotations are mainly focused on delineating the structures of interest (Valvano *et al.*, 2021). This can be effective in segmenting *regular structures* with fixed shape patterns. Hence, this task is often referred to as *regular structure segmentation*. However, such methods are challenged when applied to irregular targets with heterogeneous distributions, such as pathologies. This is also referred to as *irregular (object) segmentation*, which is particularly challenging for the medical tasks with small training datasets. Existing scribble learning approaches mainly typically focus on reconstructing complete labels from scribbles and then using the resulting pseudo labels for training. These methods include **1)** label expansion strategies that assume the pixels with similar features are likely to be in the same category (Ji *et al.*, 2019), and **2)** ensemble methods that generate labels by fusing several independent predictions (Luo *et al.*, 2022). These methods are prone to label noise from inaccurate segmentation proposals. To overcome this issue, Obukhov *et al.* (2019b) proposed a regularization loss, which exploited the similarity between labeled and unlabeled regions. Adversarial learning approach has also been applied to scribble-supervised segmentation by leveraging shape prior provided by additional full annotations (Valvano *et al.*, 2021).

Scribble-supervised segmentation generally suffers from inadequate supervision and imbalanced label classes. This often results in *under segmentation* of target structures, where the volumes of segmented structures tend to be shrunk (see Section 3.3.1). To address the problem of inadequate supervision, we first investigate the principles of generating *good scribbles*, which serve both as guidance for annotation design and as a foundation for supervision augmentation. The goal is to design efficient scribbles that maximize supervision without additional annotation costs. Our studies demonstrate that the model training benefit from the randomness of wide range distributed scribbles and larger proportion of annotated areas. Inspired by this, we propose to simulate such types of scribble-annotated images as a means of *supervision augmentation*. This can be achieved via mixup and occlusion operations on existing training images, and the supervision augmentation is coupled with regularization terms penalizing any inconsistency in the segmentation results.

Despite the lack of supervision, the scribble annotations typically have imbalanced annotated label proportions, leading to biased shape information. As a result, the model cannot accurately capture the global shape of target structures. We therefore further propose to correct the problematic prediction using prior-based regularization. This requires the critical step of estimating the mixture proportion (ratio) of each label class (referred to as π prior). We propose an algorithm to estimate this prior and use it to construct a spatial loss defined on the marginal probabilities of pixel labels and spatial energy. This spatial loss is a regularization term aimed to correct the shape of segmentation results. The supervision augmentation and prior-based regularization work in a complementary way, and both contribute to the stable and robust training on a variety of segmentation tasks.

The proposed scribble-supervised segmentation method, referred to as ZScribbleSeg, extends and generalizes the algorithms in our two preliminary works (Zhang and Zhuang, 2022a,b), and has more scientific significance in the following aspects: Firstly, we investigate principles of efficient scribble forms to guide the supervision augmentation, which have never been reported to the best of our knowledge. Secondly, we propose a new strategy leveraging spatial prior to adjust the predicted probability with computed spatial energy. Thirdly, we generalize ZScribbleSeg to the 3D cases, and validate the proposed framework on five use cases (datasets), including 3D Prostate segmentation (Decathlon-Prostate), cardiac structural segmentation (ACDC), LGE segmentation (MSCMRseg), and myocardial pathology segmentation combining three-sequence MRI (MyoPS).

The contributions of this paper are summarized as follows.

- We propose a comprehensive framework for scribble-supervised segmentation that models efficient scribbles and corrects network predictions with prior regularization. This framework aims to alleviate the problems of inadequate supervision and under-segmentation.
- To augment the supervision of scribble annotations, we first investigate the principles of efficient scribble forms. Motivated by the findings that network benefits from larger and randomly distributed annotation, we model efficient scribbles by maximizing supervision via mixup and enhancing randomness via occlusion.
- To tackle the under-segmentation and shape distortion problems, we propose a prior-guided mechanism to correct the shape of model prediction based on prior regularization, including π prior, spatial prior, and shape constraints. We utilize the EM algorithm to estimate π prior, based on which we propose the spatial prior loss to encode spatial relationship.
- Our approach achieved competitive performance in weakly supervised segmentation across diverse tasks, including regular structures in cardiac anatomy, regular structures in pathology-enhanced imaging, irregular pathological objects, and 3D prostate segmentation.

The rest of this paper is organized as follows: Section 2 briefly introduces the relevant research. In Section 3, we describe the modelling of efficient scribbles and the computation of the prior. Section 4 presents the results of the efficiency, ablation, and validation study. Finally, we conclude this work in Section 5.

2. Related work

This section provides a brief review of weakly supervised segmentation methods. Besides, we describe data augmentation strategies and regularization loss functions that are closely related to our work.

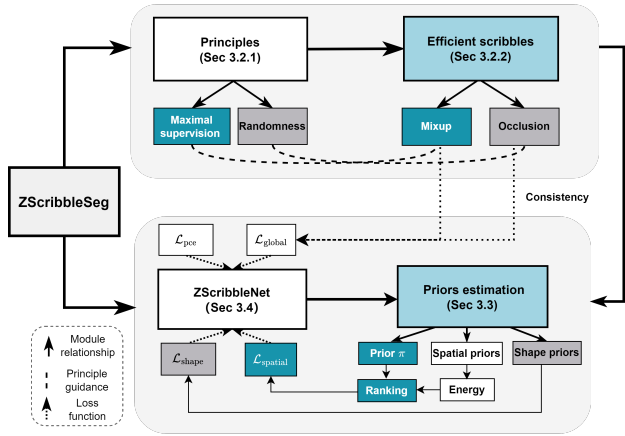


Fig. 1. Roadmap of the proposed ZScribbleSeg framework.

2.1. Weakly supervised segmentation

Recently, a variety of weakly supervised segmentation strategies have been developed to reduce the manual annotation efforts (Lin et al., 2024; Yang et al., 2024; Kweon et al., 2023; Liu et al., 2025b). Among them, the scribbles are of particular interest for the application to medical image annotation, given by their advantage in annotating nested structures. Current weakly supervised learning methods with image-level annotations mainly generate label seeds with Class Activation Map (CAM) (Zhou et al., 2016) at first, and then train the network with refined pseudo labels. However, the training of CAM requires a large scale of training data labeled with rich visual classes, which is not practical in clinical applications. Therefore, we investigate the scribble-supervised segmentation, due to its efficiency and effectiveness in both medical scenarios.

Scribble is a form of sparse annotation that provides labels for a small subset of pixels in an image (Tajbakhsh et al., 2020). Previous approaches mainly calculate losses for annotated pixels. One group of works is designed to expand the annotations and reconstruct the full label for network training. However, the expansion of labels needs to be achieved through iterative computation, which is particularly time-consuming. To alleviate it, several works removed the relabeling process and instead adopted conditional random fields to perform the refinement of segmentation results Can et al. (2018); Tang et al. (2018). However, the common issue is the unstable model training caused by noisy pseudo labels.

To obtain high-quality pseudo labels and update it throughout the training process, Luo et al. (2022) proposed to mix the predictions from a dual-branch network as auxiliary pseudo labels. This approach has achieved promising results on cardiac segmentation, but is still susceptible to inaccurate supervisions, especially on more challenging tasks with irregular objects. ScribFormer Li et al. (2024) introduces a transformer-based approach for scribble-supervised medical image segmentation. It adopts a hybrid CNNTransformer design, where CNN modules capture fine-grained local spatial details and Transformer blocks model long-range contextual dependencies. Chen et al. (2025a) addresses inconsistent and incomplete scribble annotations by constructing a reference set from class-specific to-

kens and pixel-level features and using it as a shape prior to guide pixel-level feature matching for unlabelled pixels. HELP-Net Zhang et al. (2025) introduces a hierarchical perturbation consistency module to improve feature learning via density-controlled jigsaw perturbations across global, local, and focal views, enabling multiscale structural representation learning. It further uses an entropy-guided pseudo-label module to estimate prediction confidence and generate pseudo-labels, and a structural prior refinement module that incorporates connectivity analysis and image boundary priors to refine pseudo-label quality.

Other works Valvano et al. (2021); Zhang et al. (2020) included new modules to evaluate the quality of segmentation masks, which encourages the predictions to be realistic, but requiring extra full annotations. Gao et al. (2022) introduced a weakly- and semi-supervised segmentation framework that learns from sparse scribble annotations and large unlabeled datasets using teacher-student consistency and a multi-angle projection reconstruction loss. It demonstrates strong robustness and generalization on multiple datasets. Liu et al. (2025a) combines a foreground-background separation loss and a foreground augmentation strategy with diverse context to improve foreground discrimination and generalization. Meng et al. (2023) combines superpixel-guided scribble walking for denser supervision expansion and class-wise contrastive regularization for improving class feature compactness under scribble supervision. Chen et al. (2025b) introduced Scribble2D5, a scribble-supervised 2.5D framework for volumetric segmentation that combines label propagation, boundary prediction, and an optional shape-prior module using unpaired segmentation masks. Scribbles have been also adopted for user interaction to improve the results predicted by a model. A group of studies (Asad et al., 2022; Roth et al., 2021) investigated the interactive segmentation methods based on scribbles, to refine results, accelerate training and facilitate fine-tuning.

2.2. Data augmentation

Augmentation methods are investigated to improve the model generalization ability, by synthesizing virtual training examples in the vicinity of the training dataset (Garcea et al., 2023). Common strategies include random cropping, rotation, flipping and adding noise. A line of research works have been proposed on Mixup augmentation (Qin et al., 2024; Zou et al., 2023; Zhang et al., 2018; Kim et al., 2020, 2021), which blends two image-label pairs to generate new samples for classification tasks. Input Mixup (Zhang et al., 2018) was introduced to perform linear interpolation between two images and their labels. Kim et al. (2020) proposed Puzzle Mix to leverage the saliency and local statistics to facilitate image combination. SUMix Qin et al. (2024) further proposed to learn the mixing ratio as well as the uncertainty for the mixed samples during the training process

For medical image analysis, Mixup methods have been adopted for image segmentation (Chaitanya et al., 2019) and object detection tasks (Wang et al., 2020). Although mixup operation may generate unrealistic samples, mixed soft labels can provide rich information and improve the model performance on semi-supervised segmentation (Chaitanya et al., 2019).

2.3. Regularization losses

Neural networks perform pixel-wise image segmentation, typically trained with cross-entropy or Dice loss. To predict coherent segmentation in the global sense (Kohl et al., 2018), several methods are proposed to regularize the neural network training. Here, we focus on the consistency regularization and prior regularization that most relevant to our work. In addition, Perturbation-based interpretability methods (e.g., Meaningful Perturbations (Fong Ruth, 2017) and Extremal Perturbations (Fong et al., 2019)) optimize a perturbation mask under sparsity constraints to identify evidence regions for post-hoc classifier explanations. In contrast, our method does not optimize a perturbation mask. Instead, during segmentation training, we rank a class-wise spatial energy map, use the estimated class mixture ratio (π prior) to select class-specific pixel subsets, and apply this process as a regularizer for prediction correction in scribble-supervised segmentation.

The consistency regularization leverages the fact that the perturbed versions of the same image patch should have the consistent segmentation. A series of research has been conducted on consistency regularization (Zhu et al., 2017; Ouali et al., 2020). Regularization losses have also been used in segmentation to suppress false positives and constrain prediction extent. For example, uncertainty-based background regularization can be implemented by maximizing prediction entropy over background regions, together with region-balancing constraints to avoid trivial solutions Belharbi et al. (2021). In addition, Kervadec et al. (2019); Jia et al. (2017) regularize predictions by imposing externally specified region-size constraints (e.g., target size ranges or expert-provided area estimates). In contrast, our prior regularization is designed to address class imbalance and under-segmentation by first estimating class mixture ratios (the π prior) on unlabeled pixels and then using this estimated prior to construct spatial regularization for prediction correction.

The proposed regularization of π prior is inspired from the binary mixture proportion estimation (Bekker and Davis, 2018; Garg et al., 2021; Ramaswamy et al., 2016), which was originally designed for binary (two-class) positive unlabeled learning (Du Plessis et al., 2015; Kiryo et al., 2017). For multi-class segmentation, the mixture ratios of classes are both imbalanced and inter-dependent, which cannot be solved by existing binary estimation methods.

3. Method

3.1. Overview

Problem Setup: This work investigates the scenario of scribble-supervised segmentation, where the training images are solely annotated with a small number of pixels, via scribbles for each label class.

Motivation and Strategy: To augment the supervision of scribble annotations, we first investigate different forms of scribbles. This allows us to establish principles of efficiency that maximize supervision without additional scribble effort.

These principles enable effective and robust model training with minimal annotation cost. Motivated by the principles, we introduce supervision augmentation and consistency regularization to maximize supervision while preserving global consistency. To tackle the under-segmentation problem, we further propose a prior-guided regularization scheme to exploit shape information and correct network predictions. Specifically, we first utilize the EM algorithm to estimate the class mixture ratios. Building on these estimates, we introduce a spatial prior loss by ranking spatial energy and selecting class-specific pixels. In addition, because scribble annotations are sparse, the network often produces fragmented predictions with multiple disconnected components. We therefore introduce a shape regularization term to promote inter-connectivity within the structure.

Solution: We develop ZScribbleSeg consisting of (1) modeling efficient scribbles via supervision maximization and randomness simulation; (2) modeling and computation of the priors, including label class proportion prior, spatial prior, and shape constraints; (3) integration to develop deep neural network (referred to as ZScribbleNet) having losses of partial cross entropy (\mathcal{L}_{pcc}), global consistency (\mathcal{L}_{global}), spatial prior loss ($\mathcal{L}_{spatial}$), shape regularization (\mathcal{L}_{shape}) and training strategy of supervision augmentation and prior regularization. Figure 1 presents the roadmap of the proposed framework.

3.2. Principle and modeling of efficient scribbles

We investigate the principles of efficient scribbles and derive the objective of maximizing supervision with minimal annotation efforts. This leads to the proposal of supervision augmentation. In addition, we propose a global consistency loss to penalize the non-equivalence in the augmentation.

3.2.1. Principles of efficient scribbles

We shall verify the two principles of achieving efficient scribble annotation in terms of maximal supervision later through the experiments in Section 4.2:

(1) The large proportion of pixels annotated by scribbles compared with the whole set. When the amount of annotated pixels increases, the performance of the model will gradually converge to the upper bound of full annotations. Our goal is to investigate the effective strategies to compensate for missing annotations and match the performance of full annotations.

(2) The randomness of the distribution of scribbles. This is represented by the random and wide-range annotations.

Firstly, we are motivated by the knowledge that model training benefits from the finer gradient flow through a larger proportion of annotated pixels (Tajbakhsh et al., 2020). Therefore, we try to increase the annotation proportion with same effort. One natural idea is to simply expand the width of scribbles. However, this way only increases the label amount in the local area, and lacks the ability to enlarge the annotation range across the entire image.

Secondly, we are inspired by the fact that the imaging data are easier to be restored from random samples of pixels than

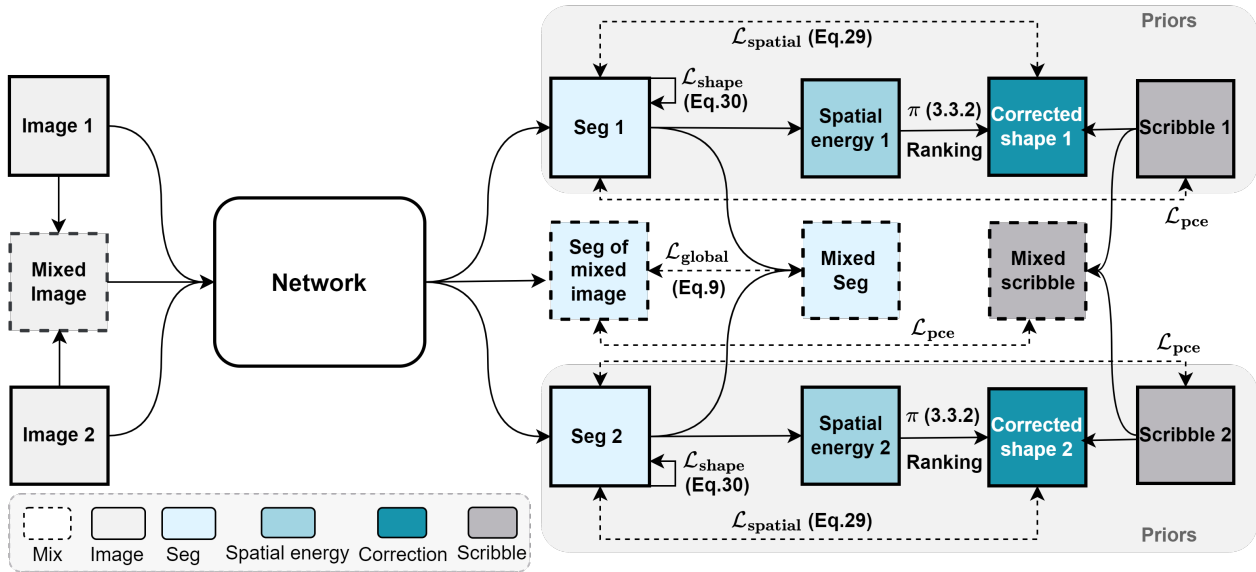


Fig. 2. Overview of the training losses for the proposed ZScribbleNet, which consists of modeling of efficient scribbles, computation of priors and shape regularization term. The scribble modeling includes mixup augmentation, regularized with global consistency ($\mathcal{L}_{\text{global}}$). The prior comprises class mixture ratios (π) and spatial prior. These components contribute to the spatial prior loss ($\mathcal{L}_{\text{spatial}}$) and the shape regularization loss

($\mathcal{L}_{\text{shape}}$). Note that spatial prior loss is complementary with the partial cross entropy loss (\mathcal{L}_{pce}) which is solely calculated for labeled pixels.

from down-sampled low-resolution images with regular patterns (Gao and Zhuang, 2020). This was due to the fact that the randomly and sparsely distributed samples maintain the global structure of the imaging data, which therefore can be restored with existing low-rank or self-similarity regularization terms. By contrast, the regularly down-sampled low-resolution images have evidently reduced tensor ranks, compared with the original high-resolution data, thus lose the global structure information. Motivated by this, we assume the features of full segmentation (similarly to the global structure information) can be portrayed (restored) with sparse scribble annotations randomly and widely distributed within the entire dataset. With such scribble annotation, the segmentation network can easily learn the global shape prior.

3.2.2. Modeling via supervision augmentation

Based on the observations that large-proportion annotated pixels and randomness of distribution lead to efficient scribbles, we propose to model efficient scribbles by supervision augmentation simulating large annotation proportion and randomness of scribble distribution. Specifically, we aim to generate training images with efficient scribbles by maximizing the supervision via mixup operations and achieving randomness via occlusion operations. To mitigate the shape distortion induced by mixup operations, we further propose a global consistency loss. This resembles data augmentation, which increases the data diversity and enables robust training.

Search optimal annotation with mixup: Motivated by the principles of efficient scribble, we first seek the optimal scribble with a large annotated ratio, high supervision, and unchanged local features. To achieve that, instead of maximizing the annotations directly, we aim to maximize the saliency of mixed

images, which measures the sensitivity of the model to inputs. Specifically, We utilize PuzzleMix (Kim et al., 2020) as the mixup operation. Given that the annotated area tends to be accompanied by high saliency, maximizing saliency also increases the scribble annotations.

We define an imagescribble pair (X, Y) as an image X together with its corresponding scribble annotation Y . We denote (X_1, Y_1) and (X_2, Y_2) are two different image-scribble pairs that are sampled independently from the training set with dimension n . We denote the resulted mixed image-label pair as (X'_{12}, Y'_{12}) . The transportation process is defined by:

$$X'_{12} = T(X_1, X_2) \text{ and } Y'_{12} = T(Y_1, Y_2),$$

$$T(X_1, X_2) = (1 - \beta) \odot \Pi_1 X_1 + \beta \odot \Pi_2 X_2,$$

where $T(X_1, X_2)$ represents the transportation process between image X_1 and X_2 ; Π_i denotes the transportation matrix of size $n \times n$ for image X_i ; β means the mask with value $[0, 1]$ of dimension n ; \odot is the element-wise multiplication. Then, we aim to maximize the saliency of transportation result over the parameters $\{\Pi_1, \Pi_2, \beta\}$:

$$\{\Pi_1, \Pi_2, \beta\} = \arg \max_{\Pi_1, \Pi_2, \beta} [(1 - \beta) \odot \Pi_1 M(X_1) + \beta \odot \Pi_2 M(X_2)],$$

where $M(X)$ denotes the saliency map of image X , which is obtained by computing the l_2 norm of gradient values. We solve this optimization problem based on PuzzleMix (Kim et al., 2020). To preserve the local statistical features, the optimization objective also includes the image local smoothness and the mixing weight prior. For details of the optimization objective, we refer readers to PuzzleMix (Kim et al., 2020) and the Section 1 of the supplementary materials.

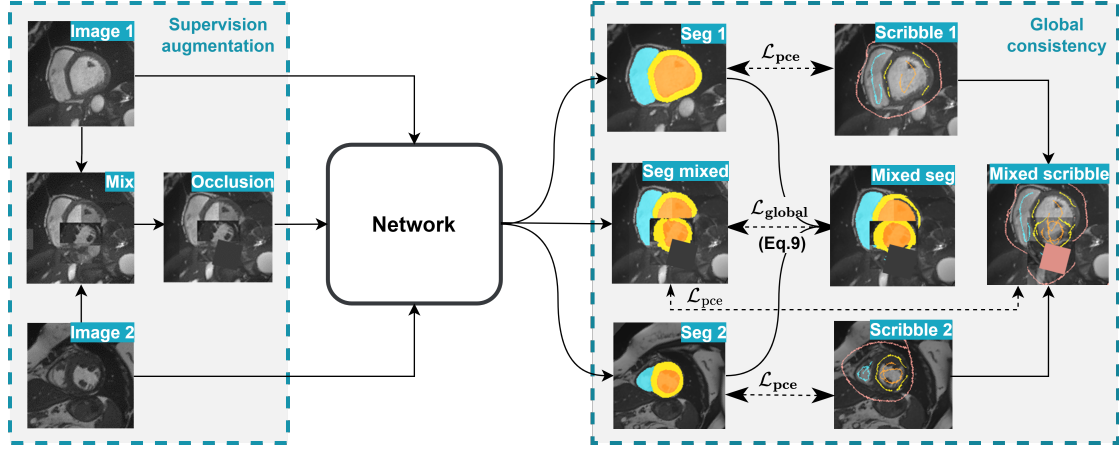


Fig. 3. Illustration of supervision augmentation and global consistency. Supervision maximization is achieved with the mix augmentation to increase the annotated proportion and data variety. Global consistency requires the segmentation result of mixed image and un-mixed image to be consistent.

Introduce randomness via occlusion: We propose to simulate randomly distributed scribbles via occlusion. Specifically, one square area of the mixed image is randomly dropped and its label is set to be the background. Since that the proportion of the background annotated by scribbles tends to be smaller than that of the foreground classes, the occlusion operation alleviates the imbalance problem of class mixture ratios within labeled pixels, and further improves the results of mixture ratio estimation, which will be elaborated in Section 3.3.2.

We denote the occluded image-label pair as (X'', Y'') , which is obtained by:

$$\begin{aligned} X''_{12} &= (1 - \mathbf{1}_b) \odot X'_{12}, \\ Y''_{12} &= (1 - \mathbf{1}_b) \odot Y'_{12}, \end{aligned}$$

where $\mathbf{1}_b$ denotes a rectangular mask of size $n \times n$ with value in $[0, 1]$. The rectangular mask is randomly rotated to occlude the mixed image, and turns the occluded area into background. Following (Yun et al., 2019), we set the size of rectangular to be 32×32 . This size is suitable for typical spatial scale of cardiac structures in 2D slices. Smaller masks introduce limited perturbation and fail to increase the diversity of labeled background pixels, whereas significantly larger masks remove too much image content and may disrupt local anatomical cues.

Global consistency loss: The objective of global consistency regularization is to leverage the mix-invariant property. As Figure 3 shows, global consistency requires the same image patch to have consistent segmentation in two scenarios, *i.e.*, the un-mixed image and the mixed image. Let the segmentation result of image X predicted by network be $\hat{Y} = f(X)$. For the transported image $X'_{12} = T(X_1, X_2)$, the consistency of mixup is formulated as:

$$T(f(X_1), f(X_2)) = f(T(X_1, X_2)),$$

which requires the segmentation of mixed image to be consistent with the mixed segmentation, after the same transportation process. When applying the occlusion operation, we further

have:

$$(1 - \mathbf{1}_b) \odot T(\hat{Y}_1, \hat{Y}_2) = f((1 - \mathbf{1}_b) \odot T(X_1, X_2)). \quad (1)$$

Then, we propose to minimize the distance between two sides of Eq.(1). Let $u_{12} = (1 - \mathbf{1}_b) \odot T(\hat{Y}_1, \hat{Y}_2)$ and $v_{12} = f((1 - \mathbf{1}_b) \odot T(X_1, X_2))$. The negative cosine similarity $\mathcal{L}_n(u_{12}, v_{12})$ is defined as:

$$\mathcal{L}_n(u_{12}, v_{12}) = -\frac{u \cdot v}{\|u_{12}\|_2 \cdot \|v_{12}\|_2}.$$

Taking the symmetrical metric into consideration, we similarly penalize the inconsistency between u_{21} and v_{21} . Therefore, the global consistency loss is formulated as:

$$\mathcal{L}_{\text{global}} = \frac{1}{2} [\mathcal{L}_n(u_{12}, v_{12}) + \mathcal{L}_n(u_{21}, v_{21})]. \quad (2)$$

Discussion: The mix operations of mixup and occlusion could change the shape of target structures, resulting in the unrealistic image. To tackle it, as Figure 3 shows, we propose to combine the partial cross entropy (PCE) loss for labeled pixels of both mixed and un-mixed images, and leverage mix equivalence to preserve shape consistency at the global level. To further exploit the shape features, we propose to correct the network prediction guided by the computed prior, which is described in Section 3.3.

3.3. Modeling and computation of the priors

To further exploit the shape features and tackle the under-segmentation problem, as Figure 1 shows, we model class mixture ratios, the spatial prior, and the shape constraints to better capture shape information and regularize the network training. As visualized in Figure 5, we compute the spatial energy to reflect the probabilities of pixels belonging to each class. We seek to estimate the critical prior of label class proportions, referred to as π , which guides the correction of erroneous network prediction.

3.3.1. Problems statement

The segmentation network trained with scribbles tends to generate under segmentation results of the target structures.

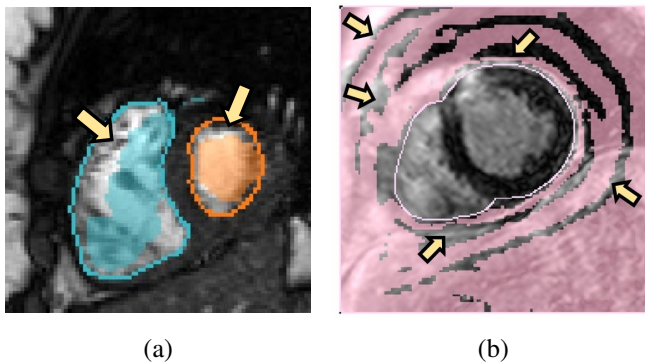


Fig. 4. Two under segmentation examples indicated by yellow arrows: (a) foreground classes (left and right ventricles) in ACDC dataset; (b) background in MyoPS dataset.

Considering that the annotated ratio of classes can be imbalanced, the scribble-supervised learning also brings challenges to the estimation of class mixture ratios π .

Imbalanced classes: Firstly, the number of pixels of different label class (denoted using n_k , where $N = \sum_{k=1}^m n_k$) in an image can be different. We denote this ratio of label class as class mixture ratios, $\pi = \{\pi_k\}_{k=1}^m$, and $n_k = N \times \pi_k$. Secondly, the ratios of scribble-annotated pixels to all the pixels of a label class, denoted as $\alpha = \{\alpha_k\}_{k=1}^m$, are generally different. In fully supervised segmentation, imbalanced classes from different class mixture ratios generally do not represent a challenge, as this ratio for each training image is known from the gold standard segmentation ($\pi_k = n_k/N$), where one can also view the annotation ratios of all labels are all equal to one, i.e., $\alpha_k = 1, k = 1, \dots, m$. However, in scribble supervision we only have information about the scribble-annotated pixels of each class in a training image. Let us denote the numbers of annotated pixels of label classes as $n_l = \{n_l^k\}_{k=1}^m$, where $n_l^k = n_k \times \alpha_k$ and $n_k = N \times \pi_k$. Without the information of either mixture ratio π_k or annotation ratio α_k , the model could not learn the coverage (number of pixels, n_k) for each class during training, thus easily leading to the phenomenon of under segmentation for certain classes.

Under segmentation: As Figure 4 shows, under segmentation refers to the results, where the size of segmented structure is generally smaller than ground truth, a phenomenon caused by the imbalanced annotated proportion and missed shape information. Note that Over-segmentation is inherently unlikely to occur in scribble-supervised settings because sparse annotations provide only positive evidence for foreground. Since unlabeled pixels are not treated as foreground, it is hard to encourage the model to expand the predicted region beyond the foreground structures during training. To solve the problem, we propose to evaluate π and the spatial prior, which are crucial for the shape refinement. The accurate estimation of π can correct the imbalanced label ratios, and enable model to adjust the size of segmentation result. The computation of spatial prior is able to encode the feature similarity between pixels, and rectify the shape of target structures. We encode π and the spatial prior with a spatial prior loss, by ranking the spatial energy and se-

lect the top π ratio as the segmentation. To estimate π , we start from the imbalanced class frequencies and adapt it from labeled pixels to unlabeled pixels.

Note that the problem of under segmentation can be even worse without the modeling of efficient scribbles. In the case of manually annotated scribbles, the resulting annotations may be distributed in a non-random pattern due to fixed labeling habits, resulting in the biased label distribution across the whole dataset. This problem could be alleviated by simulating randomly distributed labels through our proposed supervision augmentation.

Challenges of π estimation: The evaluation of class mixture ratios is a critical bottleneck in semi-/ weak-/ non-supervised learning, and serves as the basis of classes identification (Garg et al., 2021) and variance reduction (Wu and Zhuang, 2022; Sakai et al., 2017). However, existing methods are mainly proposed for binary classification, and can not be adapted to multi-class scenario directly. For segmentation task, the class mixture ratios are both imbalanced and interdependent, leading to the decrease in the performance of previous binary estimation approaches. Despite the class imbalance problem, the scribble-supervised segmentation is also faced with the imbalance of annotated class ratios. For example, the annotated ratio of the background tends to be much smaller than that of the foreground classes. The imbalance of annotated ratio further enhances the difficulty of π estimation.

3.3.2. Estimation of class mixture ratios

To mitigate under-segmentation in scribble-supervised learning, we estimate the class mixture ratios of the unlabeled pixels. Let $\pi = [\pi_1, \dots, \pi_m]$ denote the class prior over unlabeled pixels, where $\pi_k = p_u(c_k)$.

Objective: Given n_u unlabeled pixels $\mathbf{x} = [x_1, \dots, x_{n_u}]$ sampled from $p_u(\mathbf{x})$, we estimate π by maximizing the marginal likelihood of unlabeled observations:

$$\mathcal{L}(\pi) = \prod_{i=1}^{n_u} p_u(x_i) = \prod_{i=1}^{n_u} \left[\sum_{k=1}^m p_u(x_i | c_k) p_u(c_k) \right].$$

We assume that labeled and unlabeled pixels share the same class-conditional appearance distribution (Assumption 1), which is standard when scribbles are sampled without bias within each class.

Assumption 1 (Within-class density matching between labeled and unlabeled pixels). *For each class c_k , we assume*

$$p_\ell(x | c_k) = p_u(x | c_k) = p(x | c_k). \quad (3)$$

This assumption holds when scribbles are sampled at random within each class. It may be violated under habitual or non-random scribbles (e.g. always tracing only the centre lines of structures or avoiding boundary regions). Our supervision augmentation (random mixup and occlusion) could mitigate such biases by randomizing the spatial distribution of labeled pixels.

EM formulation: We follow an EM procedure (Latinne et al.,

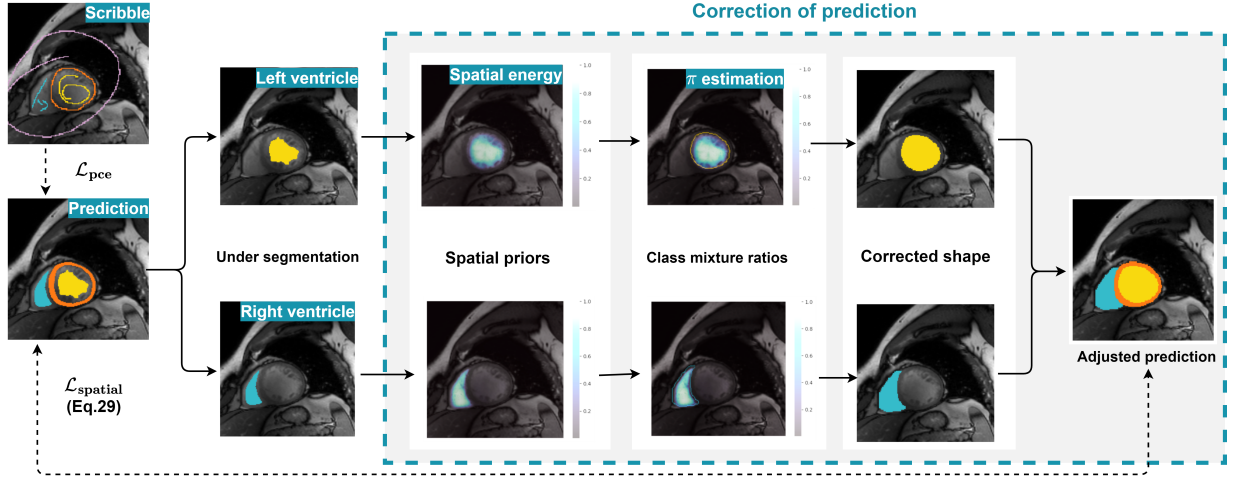


Fig. 5. Illustration of the spatial prior loss ($\mathcal{L}_{\text{spatial}}$) for correction of prediction, via class mixture ratios (π) and the spatial prior (with spatial energy).

2001; McLachlan and Krishnan, 2007) to iteratively estimate π . In the E-step, we compute the posterior responsibility of class c_k for each unlabeled pixel x_i using the current estimate $\pi^{[l]}$. Let $\hat{p}_\ell(c_k | x_i)$ denote the network prediction (posterior) and $\hat{p}_\ell(c_k)$ denote the empirical class frequency on labeled pixels. Under Assumption 1, the adapted posterior for unlabeled pixels is:

$$\hat{p}_u^{[l]}(c_k | x_i) = \frac{\pi_k^{[l]} \hat{p}_\ell(c_k | x_i) / \hat{p}_\ell(c_k)}{\sum_{j=0}^m \pi_j^{[l]} \hat{p}_\ell(c_j | x_i) / \hat{p}_\ell(c_j)}. \quad (4)$$

M-step: We then update the mixture ratio by averaging responsibilities over all unlabeled pixels:

$$\pi_k^{[l+1]} = \frac{1}{n_u} \sum_{i=1}^{n_u} \hat{p}_u^{[l]}(c_k | x_i). \quad (5)$$

We initialize $\pi^{[0]}$ with the class frequency on labeled pixels, i.e., $\hat{p}_\ell(c_k) = n_\ell^k / n_\ell$, and alternate Eq. (4) and Eq. (5) until convergence. Appendix ?? provides the complete-data likelihood, the Q -function, and the derivation of Eq. (4).

Discussion: There are two conditions of the proposed algorithm. Firstly, we assume the within-class probabilities of labeled and unlabeled pixels be the same, which means the labeled pixels should be randomly sampled based on classes. Secondly, π is initiated with the class frequency of labeled pixels. Since the annotated ratio of background is smaller than that of the foreground classes, the priori probabilities of foreground classes within unlabeled pixels tend to be over-estimated. The first problem can be tackled by modeling the efficient scribbles, to achieve the random distribution of annotations. For the second problem, by randomly occluding the image and replacing the occluded area with background, we are able to increase the ratio of background and alleviate this problem to some extent. Furthermore, we propose to address it with the marginal probability maximization, which will be explained in Section 3.3.4. Note that classical PU learning are primarily designed for binary settings and assume sample-wise independence. In our setting, the output space is multi-class, and the unlabeled set

consists of densely correlated pixels within an image. Correspondingly, existing PU learning methods for classification task cannot be directly used for multi-class segmentation. In this work, we adapt a PU-learning method nnPU (Kiryo *et al.*, 2017) to the multi-class segmentation scenario and compare our approach with nnPU. Specifically, positive samples of each class are distinguished from unlabeled pixels. And then we maximize the marginal probability of negative samples.

3.3.3. Computation of spatial energy

Given the estimated class mixture ratios, we aim to identify the unlabeled pixels by determining the probability of pixels belonging to each class. Instead of using model predictions directly, we further encode the spatial relationship to compensate the inaccurate results generated by segmentation network. Inspired by Obukhov *et al.* (2019a), we estimate the spatial energy of unlabeled pixels with energy term in a dense setting.

Firstly, we use Gaussian kernels G_{ij} to measure the distance between pixels at position i and j as:

$$G_{ij} = \exp \left\{ -\frac{(p_i - p_j)^2}{2\sigma_p^2} - \frac{(o_i - o_j)^2}{2\sigma_o^2} \right\}, \quad (6)$$

where p_i represents the position of pixel x_i ; o_i denotes the intensity feature; σ_p and σ_o are the bandwidth parameters for position and intensity information, respectively. The shallow features like intensity and position are specific to the pixel and do not rely on the network prediction. Then, the energy term ϕ_{ij} leveraging prediction \hat{y} is formulated as:

$$\phi_{ij}(\hat{y}) = G_{ij} \hat{y}_i \hat{y}_j,$$

which denotes the pairwise relationship between two pixels. This energy term connects every pixels with each other within one image. Based on $\phi_{i,j}$, we define the element of spatial energy Φ in a dense setting, i.e.,

$$\Phi_i(\hat{y}) = \sum_{j \in \Omega_i} \phi_{ij}(\hat{y}), \quad (7)$$

where $\Omega_i = \{\text{Pos}(i) - \text{Pos}(j) \leq r\}$, means the neighborhood window of radius r . Instead of taking the total energy as the regularization loss as (Obukhov et al., 2019a), we consider Φ as the spatial energy to reflect the relative probability of pixels belonging to each class.

3.3.4. Spatial prior and shape regularization losses

The spatial prior loss is computed by ranking the spatial energy and selecting the top π proportion of pixels as the segmentation. Considering that adjusting multiple structures directly can be challenging, we instead separate each foreground class from the others, and then tackle the individual structure. Given that the mixture ratios of foreground classes tend to be over-estimated, we instead leverage the accurate negative pixels filtered by estimated mixture ratios, and maximize the marginal probability of these pixels belonging to other classes.

Firstly, by ranking the spatial energy and applying the mixture ratio of each class, we are able to distinguish negative pixels from unlabeled pixels. For foreground class c_k , we rank the unlabeled pixels according to the spatial energy Φ^k of class c_k in Eq. (7). Given the estimated mixture ratio π_k , we set pixels in the top π_k proportion to be positive samples Ω_k . Correspondingly, the remaining pixels are taken as negative pixels, denoted as $\bar{\Omega}_k$. Taking over-estimated π_k into account, we believe the set of negative pixels $\bar{\Omega}_k$ is more accurate than Ω_k .

Secondly, we design the spatial prior loss ($\mathcal{L}_{\text{spatial}}$) based on maximal marginal probability of negative samples $\bar{\Omega}_k$ belonging to other classes. For each class c_k , we take it as foreground and fuse other classes except c_k into background. The fused class is denoted as \bar{c}_k . For pixel x_i in $\bar{\Omega}_k$, its marginal probability belonging to \bar{c}_k equals the sum of probabilities of the fused classes, *i.e.*, $\hat{p}(\bar{c}_k|x_i, x_i \in \bar{\Omega}_k) = \sum_{k'=1}^m [\mathbf{1}_{[k' \neq k]} \hat{p}(c_k|x_i)]$. To maximize the marginal probability of negative pixel x_i belonging to \bar{c}_k , we formulate the spatial prior loss as:

$$\mathcal{L}_{\text{spatial}} = - \sum_{k=1}^m \sum_{x_i \in \bar{\Omega}_k} \log(\hat{p}(\bar{c}_k|x_i)). \quad (8)$$

Our construction involves selecting a fixed-coverage pixel subset via sorting, which is different of region-selection mechanisms used in perturbation-based explanation methods (Fong Ruth, 2017; Fong et al., 2019). However, unlike Fong Ruth (2017); Fong et al. (2019) we do not optimize a perturbation mask nor aim at post-hoc interpretability. Instead, we rank a class-wise spatial energy map and use the estimated mixture ratio π_k to define class-specific sets, then regularize predictions through a probabilistic constraint to reduce under-segmentation under sparse scribble supervision.

The shape regularization loss. Due to insufficient supervision of scribbles, the network often produces multiple disconnected regions. To mitigate this problem, we propose $\mathcal{L}_{\text{shape}}$ to regularize the inter-connectivity within the structure. Different with the spatial prior loss, which constrains the size of the structure and the correlation between pixels. We adopt $\mathcal{L}_{\text{shape}}$ to further reduce noise and smooth boundary. It requires the model prediction to be consistent with its maximum connected area, and minimizes their cross entropy loss, *i.e.*,

Table 1. Summary of hyper-parameters used in the proposed training losses.

Notations	Description
λ_1	Weight of the global consistency loss $\mathcal{L}_{\text{global}}$.
λ_2	Weight of the spatial prior loss $\mathcal{L}_{\text{spatial}}$.
λ_3	Weight of the shape regularization loss $\mathcal{L}_{\text{shape}}$.
s_b	Side length of the occlusion mask in $\mathbf{1}_b$.
σ_p	Position bandwidth of Gaussian kernel in Eq. 6.
σ_o	Intensity bandwidth of Gaussian kernel in Eq. 6.
r	Neighborhood radius used in Eq. 7.
E_{warm}	Warm-up epochs before enabling $\mathcal{L}_{\text{spatial}}$.

$$\mathcal{L}_{\text{shape}} = - \sum_{k \in \Psi} F(\hat{Y}_k) \log(\hat{Y}_k), \quad (9)$$

where Ψ is the set of label classes with inter-connected structures; $F(\cdot)$ denotes the morphological function, and outputs the largest inter-connected area of input label. For targets that naturally contain multiple non-connected regions (e.g., multifocal lesions), $\mathcal{L}_{\text{shape}}$ should be disabled for the corresponding class, because the morphological operation $F(\cdot)$ would remove valid target regions.

3.4. ZScribbleNet

ZScribbleSeg is achieved via a deep neural network referred to as ZScribbleNet. Our goal is to develop a learning framework for scribble supervision by efficiently modeling scribbles and correcting network predictions via prior regularization. The proposed method does not depend on particular network architectures and can be directly applied to any segmentation backbone. To demonstrate the effectiveness of our method while decoupling it from architectural improvements, we adopted the UNet (Baumgartner et al., 2017) as the backbone for all experiments.

As Figure 2 shows, two images are mixed together to perform the supervision augmentation. Then, our ZScribbleNet takes the mixed images and unmixed images as the input, and output their segmentation results.

For model training, images and their scribble annotations are sampled to estimate the training objective (\mathcal{L}), which is formulated as:

$$\mathcal{L} = \mathcal{L}_{\text{pce}} + \underbrace{\lambda_1 \mathcal{L}_{\text{global}} + \lambda_2 \mathcal{L}_{\text{spatial}} + \lambda_3 \mathcal{L}_{\text{shape}}}_{\text{unsup}}, \quad (10)$$

where \mathcal{L}_{pce} is the partial cross entropy loss calculated for annotated pixels in unmixed image and mixed image. The global consistency loss $\mathcal{L}_{\text{global}}$ in Eq.(2) requires the mix equivalence for the supervision augmentation. The spatial prior loss $\mathcal{L}_{\text{spatial}}$ in Eq.(8) encodes the π prior and spatial prior; shape regularization loss $\mathcal{L}_{\text{shape}}$ in Eq.(9) leverages shape constraint. $\lambda_1, \lambda_2, \lambda_3$ are hyper-parameters to leverage the relative importance of different loss components. Table 1 summarized the hyper-parameters used in our method.

At the beginning of training, the prediction results of the model could be inaccurate, which would introduce noise to the

estimation of class mixture ratios π and spatial energy. Therefore, we warmly started training the networks with partial cross entropy loss \mathcal{L}_{pce} , global consistency loss \mathcal{L}_{global} , and shape regularization loss \mathcal{L}_{shape} for 100 epochs, and then invoked the spatial loss $\mathcal{L}_{spatial}$.

In the testing phase, the trained network predicted the segmentation results of input image directly.

4. Experiments and Results

We first introduce the materials used in our study, including four segmentation tasks, datasets, and evaluation protocols (Section 4.1). Then, we investigate a variety of scribble forms and analyze the principles of efficient scribbles (Section 4.2). Next, we perform an ablation study to assess the contribution of each component in the proposed ZScribbleSeg framework (Section 4.3). Finally, we compare ZScribbleSeg with state-of-the-art methods across diverse segmentation tasks using four open datasets (Section 4.4).

4.1. Materials

4.1.1. Tasks and datasets

Our validation covered four representative segmentation tasks: (1) cardiac ventricular segmentation of regular structures from anatomical MRI (ACDC) and abdomen organ structure segmentation from CT (BTCV), (2) regular structure segmentation from pathology-enhanced imaging with limited training samples (MSCMRseg), (3) irregular myocardial pathology segmentation (MyoPS) and brain tumor segmentation (Decathlon-BrainTumor) from multi-modality MRI (MyoPS), and (4) 3D prostate segmentation from multi-modality MRI (Decathlon).

ACDC dataset was from the MICCAI17 Automatic Cardiac Diagnosis Challenge Bernard et al. (2018). This dataset consists of short-axis cardiac images using anatomical MRI sequence (BSSFP) from 100 patients, with gold standard segmentation of cardiac ventricular structures, including left ventricle blood cavity (LV), left ventricle myocardium (MYO), and right ventricle blood cavity (RV). For experiments, we randomly divided the 100 subjects into a training set of 70 subjects, a validation set of 15 subjects (particularly for ablation study), and a test set of 15 subjects.

MSCMRseg was from the MICCAI19 Multi-sequence Cardiac MR Segmentation Challenge (Zhuang, 2019b, 2016), consisting of images from 45 patients with cardiomyopathy and the gold standard segmentation of LV, MYO and RV. We employed the 45 images of late gadolinium enhanced (LGE) MRI to evaluate the segmentation of ventricle structures. Following Yue et al. (2019), we divided the 45 images into three sets of 25 (training), 5 (validation), and 15 (test) images for all experiments. Note that this structure segmentation is more challenging than that on ACDC due to its smaller training set and pathology enhanced images.

MyoPS dataset was from MICCAI'20 Myocardial pathology segmentation Challenge (Li et al., 2022), consisting of paired images of BSSFP, LGE and T2 cardiac MRI from 45 patients. The task was to segment the myocardial pathologies, including scar and edema, which do not have regular shape or structure

thus their segmentation represents a different task to the regular structure segmentation. Following the benchmark study (Li et al., 2022), we split the data into 20 pairs of training set, 5 pairs of validation set and 20 pairs of test set.

Decathlon-Prostate dataset was released by the Decathlon challenge (Antonelli et al., 2022). The organizers released 32 paired MRI 3D volumes of two series, including transverse T2-weighted and the apparent diffusion coefficient (ADC). The ground truth segmentation of central gland and peripheral zone were also provided along with the images. We excluded two cases with missing labels of peripheral zones and split the remaining 30 paired volumes into three sets of 18(training), 6(validation) and 6(test). To avoid the deviation caused by random dataset division, we conducted 5-fold cross-validation and reported the average performance on test set.

Decathlon-BrainTumor dataset consists of 750 multiparametric-magnetic resonance images from patients diagnosed with either glioblastoma or lower-grade glioma (Antonelli et al., 2025). The Decathlon-BrainTumor dataset contains the same cases as the 2016 and 2017 Brain Tumor Segmentation (BraTS) challenges. They have a uniform resolution with a size of $240 \times 240 \times 155$. We aimed to segment two foreground classes: the tumor core and the peritumoral edema. The dataset was randomly split into 80%, 10% and 10% for training, validation and testing, respectively.

BTCV dataset comprises 47 abdominal CT acquired at the Vanderbilt University Medical Center from metastatic liver cancer patients or post-operative ventral hernia patients Landman et al. (2015). We aimed to segment three organs: the liver, spleen and stomach. Same as Decathlon-BrainTumor dataset, the BTCV dataset was randomly split into 80%, 10% and 10% for training, validation and testing, respectively.

4.1.2. Evaluation metrics

For each task, we reported the Dice score and Hausdorff Distance (HD) on each foreground class separately.

4.1.3. Pre-processing and implementation

The two dimensional slices from ACDC and MSCMR datasets were of different resolutions. Hence, we first re-sampled all images into a fixed resolution of 1.37×1.37 mm and then extracted the central patch of size 212×212 for experiments. For MyoPS, we took the paired slices of BSSFP, LGE, and T2 CMR and cropped their center patches of size 192×192 for experiments. For Prostate-Decathlon, we re-sampled all volumes to the resolution of $1.1 \times 1.1 \times 1.1$ mm. We then cropped $64 \times 64 \times 64$ center patches for each volume and take a paired patches of T2 and ADC sequences as an input. We normalized the intensity of these medical images to be zero mean and unit variance. For BTCV dataset, we re-sampled all images into a fixed resolution of 1.2×1.2 mm and resized the images to 256×256 . For Decathlon-BrainTumor dataset, we used the original image resolution for our experiments.

For random occlusion, a square area of 32×32 was randomly occluded for each image. For the estimation of spatial energy, We adopted Gaussian kernels with intensity bandwidth $\sigma_o = 0.1$, position bandwidth $\sigma_p = 6$, and kernel radius $r = 5$. The

Table 2. Efficiency analysis of scribble forms for regular structure segmentation of cardiac ventricles (ACDC dataset) and irregular segmentation of myocardial pathology (MyoPS dataset). Here, N_{scribble} and N_{pix} respectively denote the number of manual draws to generate scribble annotations and number of annotated pixels, which indicate annotation efforts; $\mathbf{d} = \{d_k\}_{k=1}^m$ is the number of manual draws (scribbles) and $n_l = \{n_l^k\}_{k=1}^m$ is the given threshold of annotation efforts (number of labeled pixels), where $d_k \ll n_l^k$ for each class k . Segmentation results are evaluated on test set and reported in Dice scores.

Methods	N_{scribble}	N_{pix}	Structural segmentation				Irregular segmentation		
			LV	MYO	RV	Avg	Scar	Edema	Avg
Skeleton	\mathbf{d}	n_l	.805±.145	.737±.095	.769±.128	.770±.126	.504±.213	.057±.022	.281±.271
Random walk	\mathbf{d}	n_l	.798±.173	.698±.153	.753±.157	.744±.165	.516±.284	.529±.123	.522±.184
DirRandomWalk	\mathbf{d}	n_l	<u>.844±.143</u>	<u>.755±.102</u>	<u>.798±.173</u>	<u>.799±.146</u>	<u>.539±.217</u>	<u>.637±.108</u>	<u>.588±.176</u>
Points	n_l	n_l	.876±.134	.801±.089	.858±.081	.845±.107	.551±.246	.638±.115	.595±.194

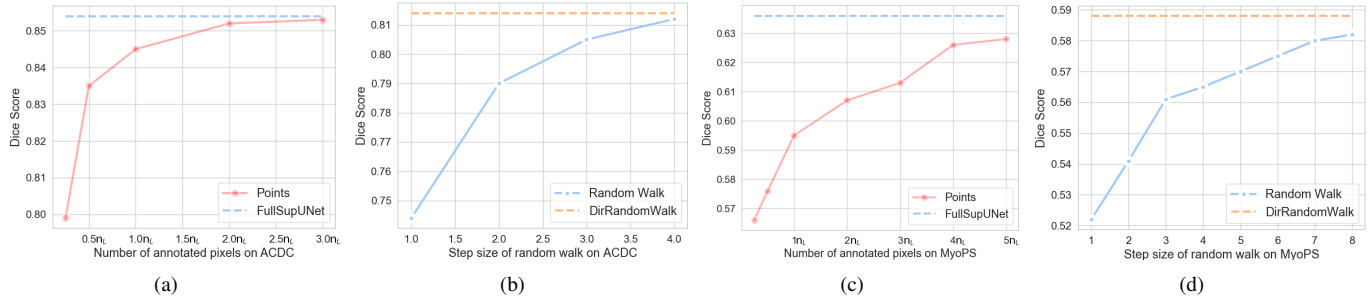


Fig. 6. Performance of segmentation networks trained using partial cross entropy computed from Points scribble form with different number of pixels N_{pix} , with comparisons to fully supervised models (FullSupUNet): (a) and (c) visualize Dice scores with respect to different N_{pix} on ACDC and MyoPS, respectively. The performance of models trained by the Random walk form, with increasing step length l , compared with models trained by DirRandWalk: (b) and (d) show the Dice scores of segmentation on ACDC and MyoPS, respectively, given $N_{\text{pix}} = n_l$.

hyper-parameters λ_1 , λ_2 , λ_3 in Eq. (10) were empirically set to be 0.05, 1, and 1, respectively.

All models were trained with a batch size of 4, learning rate of $1e^{-4}$, and augmentation of flipping and random rotation. We implemented our models with Pytorch. All models were trained on one NVIDIA 3090Ti 24GB GPU for 1000 epochs.

4.2. Efficiency of scribble forms

In this study, we first compared four scribble forms to illustrate the efficacy of randomly annotated scribbles for supervision. Denoting the number of annotated pixels using a manual and skeleton-wise scribble form as n , we generated other scribble forms with the same annotated ratios for a fair comparison. Then, we studied the performance of segmentation with respect to the number of pixels annotated using a random and wide range scribble form, by setting the number of annotated pixels to different times of n . Finally, we further explored variants of random walk annotations to show the importance of wide range in the random distribution of scribbles.

We applied two segmentation tasks, *i.e.*, regular structure segmentation of the cardiac ventricles on ACDC dataset and irregular segmentation of myocardial pathologies using MyoPS dataset. To compare the supervision of scribble forms directly, we trained all models with partial cross entropy (PCE) loss calculated for annotated pixels from scribbles. All experiment results were reported on the test set.

4.2.1. Scribble forms

Annotation effort can be assessed in two ways. One is the number of manual draws used to create scribbles (N_{scribble}), and

the other is the number of annotated pixels (N_{pix}). Given the certain amount of efforts, we designed four forms following different generation procedures, including (1) Skeleton, (2) Random walk, (3) Directed random walk (DirRandomWalk), (4) Points. The details of scribble forms are described below.

Skeleton indicates the widely adopted scribble form by a annotator, who approximately outlines the shape of each label class within the segmentation mask. For a segmentation task with m label classes, one needs \mathbf{d} manual draws (scribbles) for a training image, where $\mathbf{d} = \{d_k\}_{k=1}^m$ and $d_k \geq 1$ denotes the number of manual draws for label class k . For ACDC dataset, we adopted the manual annotated skeleton scribble released by Valvano *et al.* (2021).

Random walk starts from a random point within the segmentation mask. Then, the annotation moves along a random direction of image lattice within the segmentation mask with a given step length (l by default set to 1). We repeated such moves until the ratio or number of annotated pixels reached a threshold (n_l).

Directed random walk (DirRandomWalk) is a variant of the random walk with momentum. Scribbles generated by the standard random walk often cluster within a local region of radius \sqrt{r} after r steps. To promote broader coverage without manually specifying the step length (l), the directed random walk encourages movement in the same direction as the previous step. When the next point falls outside the segmentation mask, the direction is adjusted to the nearest feasible angle.

Points represents an idealized scribble form, where annotated pixels are randomly sampled within the segmentation mask. However, it is difficult to generate such scribble annota-

Table 3. Results in Dice scores and Hausdorff Distance (HD) of the ablation study using ACDC dataset, where the models were evaluated on the validation set. Note that model #8 is ZScribbleSeg. Bold denotes the best result, and underline indicates the best but one in each category.

Dice	\mathcal{L}_{pce}	Efficiency		\mathcal{L}_{global}	\mathcal{L}_{shape}	$\mathcal{L}_{spatial}$		LV	MYO	RV	Avg
		Mix	Occlusion			π	spatial				
model #1	✓	×	×	×	×	×	×	.863±.089	.804±.063	.774±.150	.813±.112
model #2	✓	✓	×	×	×	×	×	.871±.098	.811±.096	.771±.197	.818±.143
model #3	✓	✓	✓	×	×	×	×	.870±.100	.833±.063	.843±.076	.848±.082
model #4	✓	✓	✓	✓	×	×	×	.920±.064	.868±.051	.886±.051	.891±.059
model #5	✓	×	×	×	✓	×	×	.915±.068	.871±.056	.871±.058	.886±.064
model #6	✓	×	×	×	×	✓	×	.919±.045	.855±.050	.869±.055	.881±.057
model #7	✓	×	×	×	×	✓	✓	<u>.923±.078</u>	<u>.869±.051</u>	<u>.889±.056</u>	<u>.894±.066</u>
model #8	✓	✓	✓	✓	✓	✓	✓	.929±.057	.876±.051	.892±.049	.899±.056
HD(mm)	\mathcal{L}_{pce}	Mix	Occlusion	\mathcal{L}_{global}	\mathcal{L}_{shape}	π	$\mathcal{L}_{spatial}$	LV	MYO	RV	Avg
model #1	✓	×	×	×	×	×	×	81.86±40.40	65.97±33.62	60.91±44.62	69.58±40.37
model #2	✓	✓	×	×	×	×	×	88.88±12.42	37.18±34.04	95.01±23.32	73.69±35.85
model #3	✓	✓	✓	×	×	×	×	119.78±19.14	23.90±17.32	52.38±23.40	65.35±45.06
model #4	✓	✓	✓	✓	×	×	×	12.12±18.26	29.41±24.56	16.97±15.62	19.50±20.94
model #5	✓	×	×	×	✓	×	×	4.45±5.39	<u>15.24±23.90</u>	25.78±22.44	<u>15.16±20.89</u>
model #6	✓	×	×	×	×	✓	×	39.95±37.55	50.32±36.14	42.49±31.10	44.25±34.93
model #7	✓	×	×	×	×	✓	✓	28.95±36.57	44.77±34.69	7.51±5.34	27.08±32.76
model #8	✓	✓	✓	✓	✓	✓	✓	<u>6.09±8.53</u>	11.14±14.53	<u>8.86±5.88</u>	8.70±10.40

tion in practice, due to the huge number of manual draws which equals the number of annotated pixels, that is, $N_{scribble} = N_{pix}$. Therefore, we considered this form as the upper bound of scribble supervision under the same ratio of annotated pixels.

4.2.2. Results

Given the same amount of annotated pixels, we show the effect of different scribble forms on regular structures (ACDC) and irregular objects (MyoPS). As Table 2 illustrates, when the four scribble forms had the same number of annotated pixels N_{pix} , Points achieved the best Dice scores on both of the structural segmentation and irregular segmentation tasks. This can be attributed to the effects of randomness and wide range distribution of scribbles. However, when the annotation effort was constrained by the number of manual draws, DirRandomWalk became more favorable. In this setting, the Points form was impractical despite its superior accuracy. Furthermore, Skeleton was shown to be the least efficient form. The segmentation neural network trained on such annotation performed poorly on the irregular object segmentation task. This was due to the fact that when the target was difficult to outline, Skeleton form could fail to portray the entire segmentation. Such incomplete annotations result in poor performance or even training failure. By contrast, randomly distributed scribble forms, such as Random walk and DirRandomWalk, demonstrated clear superiority. On irregular object segmentation, they improved the average Dice score over Skeleton by 24.1% and 30.7%, respectively.

Number of annotated points: By varying the number of annotated pixels (N_{pix}), we validated the influence of annotated proportions on scribble-supervised segmentation. Figure 6 (a) and (c) show that the model performance improves as N_{pix} increases, indicating that model training benefits from a larger proportion of annotated pixels. One can observe from Figure 6 (a) that the segmentation performance started converging when N_{pix} reached $2n$. For the more difficult segmentation task on

irregular objects, the performance converged after $N_{pix} \geq 4n$. This trend is illustrated in Figure 6 (c).

Wide-ranged distribution: We further investigated the influence of a wide range distribution of scribbles with varying step length l in Random walk. As the step length increases, the label distribution range of Random walk gradually expanded. From Figure 6 (b) and (d), the average Dice score increased as the step length grew, and the performance gradually converged to that of DirRandomWalk. This confirmed that the widely distributed scribbles were better to provide finer supervision under the same number of draws and annotated pixels.

4.3. Ablation study

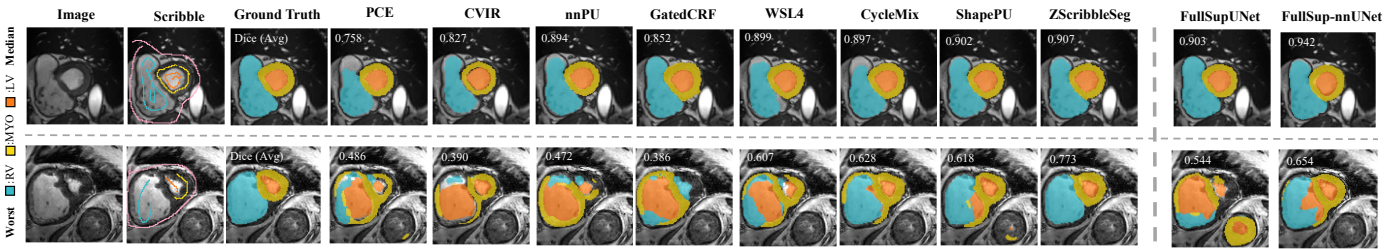
We studied the effectiveness of the proposed strategies in modeling efficient scribbles and prior regularization for ZScribbleNet. We used the ACDC dataset and the expert-made scribble annotations released by Valvano et al. (2021), and evaluated the model performance on the *validation set*.

We consider eight ablated models trained with different settings. The variants progressively enable the baseline scribble loss L_{pce} , efficiency augmentation (Mix and Occlusion), and the global consistency loss L_{global} , the shape regularization loss L_{shape} , and the spatial prior $L_{spatial}$, where $L_{spatial}$ consists of mixture-ratio estimation (π) and a spatial energy term. For example, Model #7 corresponds to $L_{pce} + L_{spatial}$ (i.e., enabling both π and the spatial term), while Model #8 is the full method (ZScribbleSeg).

Table 3 presents the results. When model #3 incorporated the proposed supervision augmentation for efficient scribble modeling (indicated by the Efficiency column), its performance improved over model #1. The average Dice score increased from 0.813 to 0.848, and the average HD decreased from 69.58 mm to 65.35 mm. Specifically, mixed augmentation brings a 0.5% marginal improvement (0.818 vs. 0.813). The mix operation increases the distribution range and annotation ratios, but may

Table 4. Results and comparisons of regular structure segmentation on ACDC dataset.

Methods	Dice				HD (mm)			
	LV	MYO	RV	Avg	LV	MYO	RV	Avg
PCE	.805±.145	.737±.095	.769±.128	.770±.126	62.55±36.04	68.30±27.77	59.62±42.62	63.40±35.76
WSL4 (Luo et al., 2022)	.890±.098	.818±.057	.863±.068	.857±.074	39.75±47.27	68.80±49.66	31.61±29.93	46.72±42.29
GatedCRF (Obukhov et al., 2019a)	.846±.157	.744±.108	.822±.111	.804±.135	37.38±46.37	22.30±15.72	20.88±11.85	26.85±30.03
MAAG (Valvano et al., 2021)	.879	.817	.752	.816	25.23	26.83	22.73	24.93
CVIR (Garg et al., 2021)	.866±.127	.797±.102	.737±.130	.800±.130	47.51±50.82	10.70±8.39	14.39±9.00	24.20±34.17
nnPU (Kiryo et al., 2017)	.862±.134	.792±.124	.829±.102	.828±.123	67.28±48.60	18.60±17.93	14.64±8.39	33.51±38.43
CycleMix (Zhang and Zhuang, 2022a)	.876±.096	.794±.083	.829±.099	.833±.098	16.60±19.90	18.04±17.78	19.09±21.44	17.91±19.57
ShapePU (Zhang and Zhuang, 2022b)	.885±.103	.806±.096	.851±.089	.848±.100	20.17±22.40	41.81±33.40	20.06±26.43	27.35±29.33
TIP25 (Chen et al., 2025a)	.894±.094	.822±.059	.873±.066	.863±.061	7.26±4.11	7.08±9.54	8.74±10.11	7.69±7.01
HELNet (Zhang et al., 2025)	.931±.043	.859±.057	.931±.041	.901±.034	5.80±3.29	2.78±2.16	3.92±6.74	3.83±3.48
ScribFormer (Li et al., 2024)	.880±.109	.794±.078	.894±.063	.856±.072	14.96±18.25	17.38±19.99	13.48±8.03	15.27±13.33
ZScribbleSeg	.900±.065	.825±.069	.862±.102	.862±.086	7.69±6.94	8.93±6.40	12.74±12.48	9.79±9.19
FullSupUNet (Baumgartner et al., 2017)	.882±.123	.824±.099	.856±.112	.854±.113	11.94±13.58	12.65±12.52	14.82±9.69	13.14±11.97
FullSup-nnUNet (Isensee et al., 2021)	.903±.082	.817±.097	.902±.063	.874±.091	7.71±9.83	7.81±7.61	5.15±2.64	6.89±7.36

**Fig. 7. Visualization of cardiac segmentation on ACDC dataset. The two slices were from the median and the worst cases by the average Dice scores of all compared methods.**

change the shape of target structure. Therefore, it can be difficult for the segmentation model to learn the shape prior, leading to the HD increase in some structures. This problem is alleviated when combined with the global consistency loss, which helps preserve the shape information. In addition, the occlusion strategy increased the average Dice score by 3.0% (0.848 vs. 0.818) by enhancing annotation diversity.

When supervision augmentation was combined with the global consistency loss ($\mathcal{L}_{\text{global}}$) in model #4, the performance was further enhanced. The average Dice score increased by 4.3% (0.891 vs. 0.848), and the average HD was reduced by more than 45 mm (19.50 mm vs. 65.35 mm). Alternatively, when inter-connectivity was enforced through the shape regularization loss ($\mathcal{L}_{\text{shape}}$), model #5 achieved a dramatic reduction in HD, from 69.58 mm to 15.16 mm compared with model #1. We next examined the effect of incorporating the spatial prior ($\mathcal{L}_{\text{spatial}}$) into ZScribbleNet. Model #7, which added this single loss, achieved the largest Dice improvement of 8.1% (0.894 vs. 0.813). In particular, when only the estimated class mixture ratio π was applied, model #6 still obtained a notable gain of 6.8%. When combined with the computed spatial energy, model #7 further improved the Dice score from 88.1% to 89.4%, and reduced the average HD from 44.25 mm to 27.08 mm, demonstrating the effectiveness of incorporating the spatial prior. Finally, our ZScribbleSeg (model #8) achieved the best performance with an average Dice of 0.899 and HD of 8.70 mm. This indicated that the combination of efficient scribbles and priors endowed the algorithm with substantial supervision and prior knowledge for scribble-supervised segmentation.

4.4. Performance and Comparisons

We conducted experiments over the six segmentation tasks stated in Section 4.1. (1) For the structural segmentation of cardiac ventricles from ACDC dataset, we used the expert-made scribbles released by Valvano et al. (2021). (2) For the cardiac structural segmentation from pathology enhanced imaging (MSCMRseg) dataset, we used the manually annotated scribbles released by Zhang and Zhuang (2022a). (3) For the irregular myocardial pathology segmentation from MyoPS dataset, we first adopted the standard skeletonization algorithm for the simulated scribble annotation of pathologies Rajchl et al. (2017). Then, we manually annotated skeleton scribbles for the structures of LV, Myo, RV and background. (4) For the 3D Prostate-Decathlon dataset, we randomly select about 3-5 slices for each category in each dimension to manually label scribbles. (5) For Decathlon-BrainTumor and BTCV, we generated pseudo-scribbles on axial slices using a script designed to imitate human drawing behavior (Luo et al., 2022).

We compared ZScribbleSeg with thirteen methods. We first implemented the PCE loss (\mathcal{L}_{pce}) as a baseline method (referred to PCE). We reported results of state-of-the-art scribble-supervised methods, including HELNet (Zhang et al., 2025), TIP25 (Chen et al., 2025a), ScribFormer (Li et al., 2024), WSL4 (Luo et al., 2022), GatedCRF (Obukhov et al., 2019a), CycleMix (Zhang and Zhuang, 2022a), and ShapePU (Zhang and Zhuang, 2022b). MAAG (Valvano et al., 2021) was included on ACDC with results taken from the original paper. Note that for the MSCMRseg dataset, the test sets used

Table 5. Results and comparisons of regular structure segmentation on pathology enhanced images (LGE CMR) using MSCMRseg dataset. Note that the results of HELPNet and ScribFormer are taken from their original papers, and it can be difficult to conduct a fair cross-study comparison due to the differences in training strategies and hardware environments.

Methods	Dice				HD (mm)			
	LV	MYO	RV	Avg	LV	MYO	RV	Avg
PCE	.514±.078	.582±.067	.058±.023	.385±.243	259.4±14.19	228.1±21.36	257.4±12.43	248.3±21.63
WSL4 (Luo et al., 2022)	.902±.040	.815±.033	.828±.101	.848±.076	55.95±4.88	42.07±13.48	<u>32.08±6.57</u>	43.37±31.04
GatedCRF (Obukhov et al., 2019a)	.917±.044	.825±.032	.848±.073	.863±.066	25.72±4.37	37.92±5.10	32.83±5.59	32.16±7.11
CVIR (Garg et al., 2021)	.331±.076	.371±.088	.404±.110	.368±.095	259.2±14.23	243.0±13.76	180.9±55.44	227.7±47.63
nnPU (Kiryo et al., 2017)	.341±.067	.538±.081	.432±.100	.437±.115	259.4±14.19	201.6±66.98	199.7±57.50	220.2±57.70
CycleMix (Zhang and Zhuang, 2022a)	.748±.064	.730±.047	.835±.041	.771±.069	224.59±35.27	<u>28.26±20.77</u>	73.36±51.39	108.74±92.65
ShapePU (Zhang and Zhuang, 2022b)	.880±.046	.785±.080	.833±.087	.833±.082	178.02±50.93	178.05±25.39	189.35±55.78	181.81±45.27
TIP25 (Chen et al., 2025a)	.901±.054	.823±.087	<u>.873±.091</u>	.866±.083	<u>23.33±26.28</u>	25.42±27.60	30.60±37.23	26.45±23.67
HELPNet (Zhang et al., 2025)	.932±.040	.861±.040	.896±.040	.896	-	-	-	-
ScribFormer (Li et al., 2024)	.896	.807	.813	.839	-	-	-	-
ZScribbleSeg	<u>.922±.039</u>	<u>.834±.039</u>	.854±.055	<u>.870±.058</u>	12.10±14.70	16.52±19.14	51.03±39.27	<u>26.55±31.39</u>
FullSupUNet (Baumgartner et al., 2017)	.909±.049	.821±.054	.826±.087	.852±.076	10.02±12.36	11.89±11.34	56.91±41.99	26.27±33.63
FullSup-nnUNet (Isensee et al., 2021)	.940±.034	.880±.027	.902±.047	.907±.044	9.10±17.10	10.57±11.81	11.36±11.50	10.34±13.76

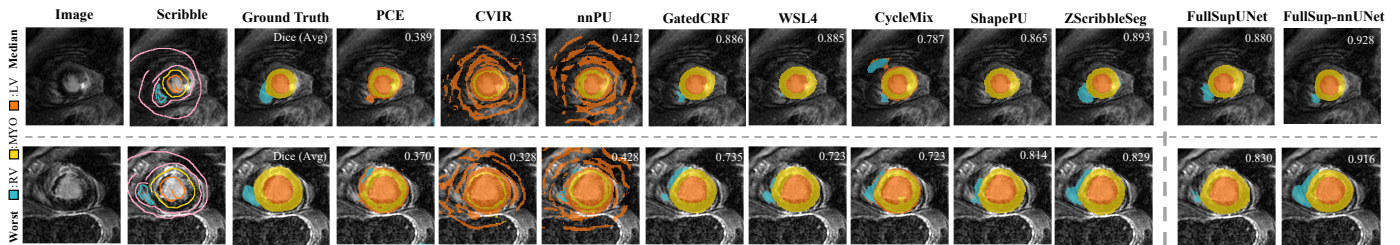


Fig. 8. Visualization of cardiac segmentation on LGE CMR using MSCMRseg dataset. The two slices were from the median and the worst cases by the average Dice scores of all compared methods.

Table 6. Results and comparisons of regular structure segmentation on BTCV dataset.

Methods	Dice				HD (mm)			
	Spleen	Liver	Stomach	Avg	Spleen	Liver	Stomach	Avg
PCE	.384±.091	.855±.021	.725±.081	.655±.226	213.93±17.98	68.61±19.89	100.68±31.85	127.74±15.18
WSL4 (Luo et al., 2022)	.584±.091	.920±.015	.818±.059	.774±.037	115.58±19.81	31.50±10.33	49.64±24.89	65.67±12.01
GatedCRF (Obukhov et al., 2019b)	.608±.095	.919±.021	.825±.060	.783±.042	109.10±20.14	44.97±20.93	35.49±39.91	63.21±14.23
CVIR (Garg et al., 2021)	.596±.072	.829±.046	.724±.099	.716±.058	112.96±36.4	77.88±25.96	102.56±30.04	97.80±26.05
nnPU (Kiryo et al., 2017)	.557±.101	.915±.027	.809±.063	.760±.045	128.65±19.25	34.76±15.05	75.59±21.45	79.67±18.56
CycleMix (Zhang and Zhuang, 2022a)	.738±.074	.922±.097	.823±.091	.827±.095	89.09±16.72	29.35±12.88	32.52±21.39	50.32±19.63
ShapePU Zhang and Zhuang (2022b)	.745±.092	.926±.067	.819±.076	.830±.081	76.09±25.45	25.29±10.18	48.43±24.23	49.94±23.12
TIP25 (Chen et al., 2025a)	.780±.066	.932±.080	.837±.075	.850±.073	49.88±10.73	20.15±13.28	22.82±15.31	30.95±14.22
HELPNet (Zhang et al., 2025)	.796±.045	.940±.088	.842±.090	.859±.075	36.48±9.43	<u>18.97±5.34</u>	<u>21.31±8.27</u>	<u>25.59±8.42</u>
ScribFormer (Li et al., 2024)	.752±.175	.930±.212	.821±.370	.834±.379	62.54±13.87	21.97±10.34	33.38±15.27	39.30±14.57
ZScribbleSeg	<u>.784±.034</u>	.947±.012	<u>.839±.066</u>	<u>.856±.080</u>	<u>38.39±4.30</u>	12.17±6.83	17.72±5.35	22.76±6.32
FullSupUNet (Baumgartner et al., 2017)	.825±.046	.961±.032	.867±.044	.884±.076	23.72±5.44	4.31±1.33	10.81±6.46	12.95±6.10
FullSup-nnUNet (Isensee et al., 2021)	.838±.039	.968±.045	.875±.069	.893±.062	19.46±4.89	4.24±0.98	10.25±4.46	11.31±5.19

Table 7. Results and comparisons of irregular segmentation of myocardial pathologies on MyoPS dataset.

Methods	Dice			HD (mm)		
	Scar	Edema	Avg	Scar	Edema	Avg
PCE	0.504±0.213	0.057±0.022	0.281±0.271	82.68±33.95	147.61±20.59	115.15±43.00
WSL4 (Luo et al., 2022)	-	-	-	-	-	-
GatedCRF (Obukhov et al., 2019b)	-	-	-	-	-	-
CVIR (Garg et al., 2021)	0.505±0.214	0.080±0.031	0.293±0.263	61.59±32.09	125.27±20.83	93.43±41.86
nnPU (Tarvainen and Valpola, 2017)	0.530±0.241	0.085±0.035	0.308±0.282	48.88±23.55	125.27±20.83	87.07±44.47
CycleMix (Zhang and Zhuang, 2022a)	0.550±0.237	0.626±0.124	0.588±0.191	65.64±42.81	81.97±40.87	73.81±42.13
ShapePU (Zhang and Zhuang, 2022b)	0.558±0.237	0.615±0.144	0.587±0.205	57.33±31.58	53.00±31.42	55.16±31.17
TIP25 (Chen et al., 2025a)	0.603±0.175	0.652±0.141	0.628±0.193	49.29±20.31	50.23±22.56	49.76±21.44
HELPNet (Zhang et al., 2025)	0.611±0.204	0.655±0.147	0.633±0.186	45.89±20.12	47.74±21.34	46.82±20.89
ScribFormer (Li et al., 2024)	0.571±0.266	0.648±0.190	0.610±0.228	50.55±19.09	51.28±24.21	50.92±21.65
ZScribbleSeg	0.596±0.237	0.676±0.113	0.636±0.188	46.73±20.04	47.05±24.30	46.89±21.98
FullSupUNet (Baumgartner et al., 2017)	0.607±0.253	0.659±0.135	0.633±0.202	55.35±35.73	63.53±33.15	59.44±34.27
FullSup-nnUNet (Isensee et al., 2021)	0.610±0.169	0.651±0.246	0.630±0.209	33.89±14.00	32.55±17.88	33.22±15.87

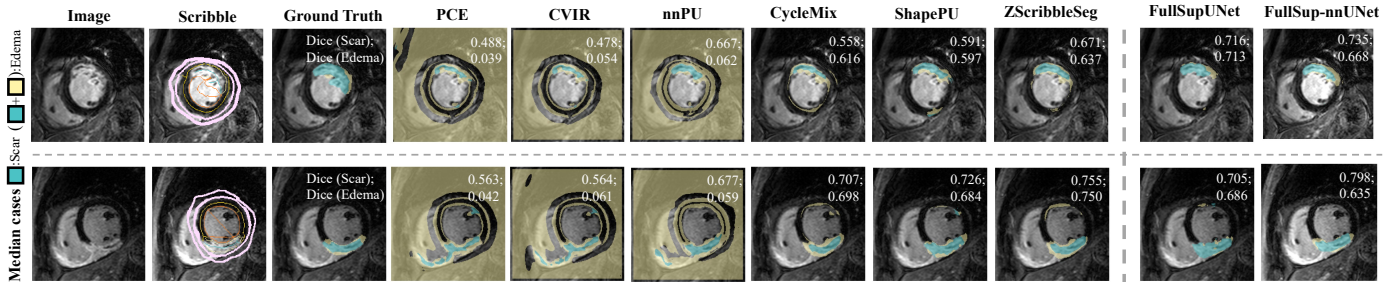


Fig. 9. Visualization of irregular segmentation of myocardial pathologies on MyoPS dataset. The two slices were from the median cases by average Dice scores of edema or scar segmentation of all compared methods.

Table 8. Results and comparisons of irregular structure segmentation using Decathlon-BrainTumor dataset.

Methods	Dice			HD (mm)		
	Tumor	Edema	Avg	Tumor	Edema	Avg
PCE	0.683±0.215	0.569±0.312	0.626±0.288	89.84±42.16	68.13±31.54	78.99±38.86
WSL4 (Luo et al., 2022)	0.709±0.235	0.669±0.167	0.689±0.188	76.29±31.24	63.28±27.23	69.79±28.34
GatedCRF (Obukhov et al., 2019a)	0.713±0.244	0.670±0.297	0.692±0.284	74.38±29.24	60.51±21.60	67.45±25.36
CVIR (Garg et al., 2021)	0.720±0.265	0.667±0.343	0.694±0.279	71.15±38.43	59.42±24.30	65.29±28.41
nnPU (Kiryo et al., 2017)	0.708±0.350	0.648±0.389	0.678±0.364	80.49±34.27	66.29±26.70	73.39±29.16
CycleMix (Zhang and Zhuang, 2022a)	0.741±0.389	0.711±0.236	0.726±0.253	38.56±25.82	37.55±21.57	38.10±23.88
ShapePU (Zhang and Zhuang, 2022b)	0.750±0.296	0.712±0.236	0.731±0.272	33.29±19.42	30.16±17.57	31.73±18.13
TIP25 (Chen et al., 2025a)	0.784±0.077	0.724±0.078	0.754±0.081	21.82±13.94	21.88±10.45	21.85±12.64
HELPNet (Zhang et al., 2025)	0.811±0.054	0.734±0.086	0.772±0.077	20.69±12.66	19.57±9.10	20.13±10.98
ScribFormer (Li et al., 2024)	0.773±0.086	0.720±0.109	0.747±0.090	27.28±9.38	24.81±14.83	26.05±13.22
ZScribbleSeg	0.788±0.089	0.737±0.098	0.763±0.098	24.28±12.13	19.91±8.14	22.10±10.67
FullSupUNet (Baumgartner et al., 2017)	0.803±0.097	0.821±0.156	0.812±0.112	21.34±4.87	12.38±5.63	16.86±5.38
FullSup-nnUNet (Isensee et al., 2021)	0.816±0.078	0.829±0.218	0.823±0.191	18.87±5.69	11.01±4.67	14.94±4.97

by HELPNet and ScribFormer are the same as ours. Therefore, we also report the results of their original papers. Furthermore, we considered semi-supervised methods based on positive-unlabeled learning, namely CVIR (Garg et al., 2021) and nnPU (Kiryo et al., 2017). We re-implemented both for scribble-supervised segmentation. Finally, we trained UNet and nnUNet with full annotations as the baselines of fully-supervised approach (referred to as FullSupUNet and FullSup-nnUNet, respectively). For the details of compared methods, please refer to the Section 2 of the supplementary materials.

4.4.1. Structure segmentation from anatomical images

Table 5 presents the Dice and HD results of 11 approaches for regular structure segmentation of cardiac ventricles from ACDC dataset. One can observe that ZScribbleSeg achieved an average Dice of 0.862, while TIP25, HELPNet, and ScribFormer obtained higher Dice scores of 0.863, 0.901, and 0.856, respectively. We further evaluate regular abdominal organ segmentation on the BTCV dataset. As Table 6 shows, among all compared methods, HELPNet obtained highest average Dice (0.859) and spleen HD, while ZScribbleSeg achieved an average Dice of 0.856 and the lowest average HD of 22.76 mm. Particularly, the HD results of ZScribbleSeg were better than the other methods except on the spleen. Note that HD is highly sensitive to the noisy and outlier segmentation results, which are commonly seen when the supervision of global shape information is not sufficient. The results indicate the proposed efficient scribble modeling and prior regularization were able to alleviate the problem of inadequate supervision and incomplete

shape information from training images with scribble annotations. Finally, Figure 7 visualizes two typical cases (median and worst) of ACDC dataset for illustration.

4.4.2. Structure segmentation from pathology enhanced images

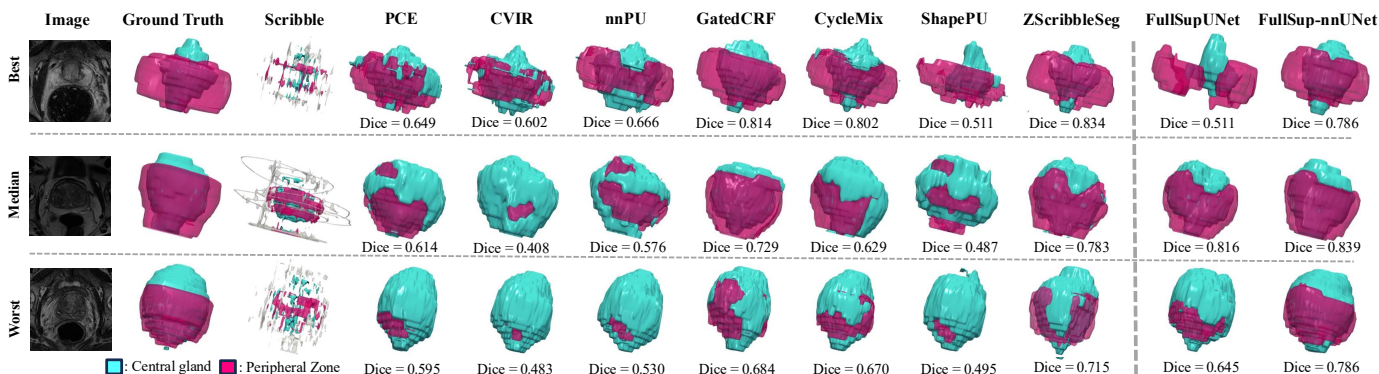
The anatomical segmentation from pathology-enhanced images was more challenging than that of the ACDC dataset. This is mainly because MSCMRseg provides fewer training subjects (25 vs. 70) and the LGE CMR images exhibit lower quality and more complex appearance patterns.

Table 5 provides the quantitative results, and Figure 8 visualizes two special examples (median and worst) for demonstration. ZScribbleSeg achieved promising performance with an average Dice of 0.870 and HD of 26.55 mm, which are the second best performance among all compared method. Notice that for this particular challenging task, the two general semi-supervised methods, CVIR and nnPU, failed to work properly, as evidenced by the unsuccessful segmentation examples shown in Figure 8.

Finally, similar to the results in previous study (Section 4.4.1), ZScribbleSeg and FullSupUNet could achieve less noisy segmentation. This was confirmed by their substantially better HD results in Table 6. Hence, we conclude that ZScribbleNet benefits from substantially augmented supervision and global shape information through the proposed efficient scribble modeling and prior regularization.

Table 9. Results and comparisons of 3D segmentation on Decathlon Prostate dataset with 5-fold cross validation. The results were reported on the test set.

Methods	Dice			HD (mm)		
	Central gland	Peripheral Zone	Avg	Central gland	Peripheral Zone	Avg
PCE	0.784±0.138	0.535±0.190	0.659±0.213	19.85±15.58	25.73±12.72	22.79±15.31
WSL4 (Luo et al., 2022)	-	-	-	-	-	-
GatedCRF Obukhov et al. (2019b)	0.776±0.112	0.555±0.177	0.666±0.123	31.90±21.82	31.41±117.40	31.66±18.43
CVIR (Garg et al., 2021)	0.780±0.139	0.518±0.222	0.649±0.238	<u>15.26±10.37</u>	22.93±9.94	19.10±11.17
nnPU (Tarvainen and Valpola, 2017)	0.779±0.133	0.529±0.196	0.654±0.218	19.29±12.29	23.49±10.21	21.39±11.81
CycleMix (Zhang and Zhuang, 2022a)	<u>0.796±0.159</u>	0.583±0.218	<u>0.689±0.229</u>	17.31±15.48	21.44±11.47	19.37±14.01
ShapePU (Zhang and Zhuang, 2022b)	0.792±0.180	<u>0.587±0.243</u>	<u>0.689±0.240</u>	15.46±10.87	<u>23.15±13.09</u>	19.31±12.90
ZScribbleSeg	0.799±0.142	0.612±0.204	0.706±0.207	14.81±8.82	23.76±18.26	<u>19.28±14.93</u>
FullSupUNet (Baumgartner et al., 2017)	0.776±0.138	0.547±0.185	0.661±0.212	15.37±12.19	19.18±12.38	17.28±13.14
FullSup-nnUNet (Isensee et al., 2021)	0.845±0.095	0.607±0.252	0.726±0.225	8.57±2.77	19.17±14.25	13.87±11.30

**Fig. 10. Visualization of results on Prostate dataset. The selected subjects were the best, median and worst cases by the average Dice scores of all compared methods.**

4.4.3. Irregular pathology segmentation

For segmentation of objects with heterogeneous shape features, it becomes particularly challenging to learn the accurate shape information for inference. We evaluated ZScribbleSeg on such challenging task of irregular segmentation using myocardial pathology segmentation (MyoPS) and Decathlon-BrainTumor datasets, where *we removed the shape regularization term \mathcal{L}_{shape} due to the nature of pathologies lacking such property.*

Table 7 presents the detailed performance results. Figure 9 further illustrates two representative cases, namely the median examples in terms of average Dice scores for edema and scar segmentation. One can find that the advantages of the proposed methodologies were demonstrated in such challenging task. ZScribbleSeg achieved the highest average Dice (0.636), while HELPNET and TIP25 also obtained promising performance with average Dice 0.633 and 0.628, respectively. The performance gains of ZScribbleSeg, either in terms of Dice or HD, were significant from CycleMix, ShapePU and finally to ZScribbleSeg compared to PCE, WSL4, GatedCRF, CVIR and nnPU ($p < 0.001$). In fact, the five compared methods failed to segment edema, and both WSL4 and GatedCRF also failed on scar segmentation. This is illustrated in the visualized examples in Figure 9. Although WSL4 and GatedCRF performed well with scribble supervision in the two regular structure segmentation tasks, they suffered severely from noisy labels in this setting. Their reliance on pseudo labels made the training un-

stable and led to model failure. The difficulty is exacerbated by the similar texture of edema and surrounding tissues across imaging modalities. Without robust estimation and regularization of class mixture ratios, accurate delineation becomes infeasible, leading to the universal failure of the compared methods. By contrast, ZScribbleSeg succeeded in this task thanks to their own methods of estimating the class prior π and applying spatial regularization. This is confirmed by their averaged HD results on scar and edema, with ShapePU at 55.16 mm and ZScribbleSeg further reduced to 46.89 mm. Table 8 reports the quantitative results for tumor core and peritumoral edema segmentation. ZScribbleSeg achieved second best performance in terms of Dice, with an average Dice of 0.763. These results further support the robustness of the proposed framework on more challenging irregular pathology segmentation tasks.

4.4.4. 3D Segmentation

We generalized ZScribbleSeg to 3D cases and validated the proposed framework on the 3D Prostate segmentation (Decathlon-Prostate) sequences. Table 9 summarizes the Dice and HD results of 9 methods. Since the released code of WSL4 (Luo et al., 2022) is designed for 2D images, we did not include it for this study. The proposed ZScribbleSeg obtained the average Dice score of 0.726 and HD of 19.28 mm, surpassing the result of other scribble-supervised methods. We provided detailed results of compared methods on each fold in the Section 3 of the supplementary material.

Figure 10 presents three typical cases, including the best, the

Table 10. Runtime and peak GPU memory with/without L_{spatial} on ACDC (2D), MyoPS (2D) and Prostate (3D). Inference time is reported per volume for per 2D image and 3D volume.

Dataset	Dim.	Input	Patch size	L_{spatial}	Train		Inference	
					Time (s/iter)	Mem (GB)	Time (s)	Mem (GB)
ACDC	2D	1-ch	212×212	w/o	0.1423	2.658	0.0061	2.434
				with	0.1689	2.671	0.0061	2.434
MyoPS	2D	3-ch	192×192	w/o	0.1618	3.410	0.0073	2.473
				with	0.1935	3.421	0.0073	2.473
Prostate	3D	1-ch	$64 \times 64 \times 64$	w/o	0.4823	6.850	0.1344	4.850
				with	0.5202	6.904	0.1344	4.850

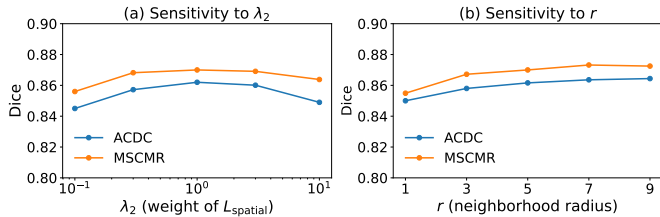


Fig. 11. Sensitivity analysis of key hyperparameters on ACDC and MSCMRseg. We vary the spatial prior weight λ_2 and the neighborhood radius r , while keeping all other settings fixed.

median, and the worst results selected by the average dice score of all compared methods. ZScribbleSeg generated segmentations with more realistic shape and size than the other scribble based methods, and this advantage was particularly evident for peripheral zone segmentation.

4.4.5. Scalability and Parameter Sensitivity Analysis

Table 10 reports the training and inference time together with the peak GPU memory usage with and without L_{spatial} on two 2D datasets (ACDC and MyoPS) and one 3D dataset (Prostate). Enabling L_{spatial} introduces a moderate training overhead, as it requires computing the spatial energy Φ and performing local ranking and top- π selection. Specifically, the training time increases from 0.1423 to 0.1689 s/iter on ACDC, from 0.1618 to 0.1935 s/iter on MyoPS, and from 0.4823 to 0.5202 s/iter on Prostate. The corresponding increase in peak training memory is marginal. In contrast, inference time and memory remain unchanged across all datasets, since the Φ -based ranking is only used during training and the test-time forward pass is identical to the baseline model. Although Φ can be expressed in a dense pairwise form, in practice it is computed locally within a radius- r neighborhood (Eq. 7), rather than over all pixel pairs. As a result, the computational complexity scales as $\mathcal{O}(N \cdot r^2)$ in 2D (and $\mathcal{O}(N \cdot r^3)$ in 3D), where N denotes the number of pixels and r the neighborhood radius. Increasing r enlarges the local window and thus increases the constant factor of the computation quadratically, but does not change the linear asymptotic complexity with respect to image size. Figure 11 further illustrates the sensitivity to the spatial prior weight λ_2 and the neighborhood radius r on ACDC and MSCMRseg. The performance is stable across a broad range of λ_2 values. Increasing r improves Dice scores initially and then saturates.

5. Conclusion

In this work, we proposed ZScribbleSeg, a new framework for scribble-supervised segmentation that integrates efficient scribbles and prior regularization within a deep neural network (ZScribbleNet). ZScribbleSeg leverages the principles of effective scribble annotations and augments scribble supervision in ZScribbleNet through mixupocclusion operations and global consistency regularization. Then, we explored to capture the global information by incorporating the prior information, particularly with proposals of the spatial prior loss. This loss was based on the estimated spatial energy and label class mixture proportions π . The former provides a new means to identify the probability of unlabeled pixels belonging to each class without directly using model predictions; The latter was developed based on the EM algorithm and was aimed to correct the problematic prediction via the regularization of the spatial prior loss.

To evaluate the performance of ZScribbleSeg, we investigated a variety of segmentation tasks, including regular structural segmentation of cardiac ventricles from anatomical imaging data (using ACDC dataset), regular structural segmentation of pathology enhanced imaging data (MSCMRseg), irregular object segmentation from multi-modality imaging (MyoPS) and 3D prostate segmentation from multi-modality imaging (Decathlon-Prostate). Compared with existing scribble-supervised approaches, ZScribbleSeg demonstrates superior performance. With augmented supervision and prior regularization, ZScribbleSeg performed reliably in challenging scenarios. It showed strong generalizability on small training sets (MSCMRseg) and irregular structure segmentation (MyoPS), where other compared methods failed.

Free-form weak annotations include points, bounding boxes, and textual descriptions in addition to scribbles. In this work, we focused solely on scribble supervision. In practice, the supervision may take different forms due to the variety of annotations that exist in hospital filing systems. Moreover, training segmentation networks for rare diseases remains challenging, particularly for irregular pathological objects due to the extremely limited data. Hence, future work will explore supervision augmentation and prior estimation for weakly supervised segmentation in rare disease scenarios. This will involve combining multiple forms of free-form annotations.

Acknowledgment

This work was funded by the National Natural Science Foundation of China (grant No. 62372115) Shanghai Municipal Education Commission-Artificial Intelligence Initiative to Promote Research Paradigm Reform and Empower Disciplinary Advancement Plan (grant no. 24KXZNA13) Shanghai Oriental Elite Talent (YingCai) Program.

References

- Antonelli, M., Reinke, A., Bakas, S., Farahani, K., Kopp-Schneider, A., Cardoso, M.J., 2025. The medical segmentation decathlon. *Medical Image Analysis* 102, 103572.

- Antonelli, M., Reinke, A., Bakas, S., Farahani, K., Kopp-Schneider, A., Landman, B.A., Litjens, G., Menze, B., Ronneberger, O., Summers, R.M., et al., 2022. The medical segmentation decathlon. *Nature communications* 13, 4128.
- Asad, M., Fidon, L., Vercauteren, T., 2022. Econet: Efficient convolutional online likelihood network for scribble-based interactive segmentation. *International Conference on Medical Imaging with Deep Learning*, 35–47.
- Baumgartner, C.F., Koch, L.M., Pollefeys, M., Konukoglu, E., 2017. An exploration of 2d and 3d deep learning techniques for cardiac mr image segmentation. *International Workshop on Statistical Atlases and Computational Models of the Heart*, 111–119.
- Bekker, J., Davis, J., 2018. Estimating the class prior in positive and unlabeled data through decision tree induction. *AAAI Conference on Artificial Intelligence* 32.
- Belharbi, S., Rony, J., Dolz, J., Ayed, I.B., McCaffrey, L., Granger, E., 2021. Deep interpretable classification and weakly-supervised segmentation of histology images via max-min uncertainty. *IEEE transactions on medical imaging* 41, 702–714.
- Bernard, O., Lalonde, A., Zotti, C., Cervenansky, F., Yang, X., Heng, P.A., Cetin, I., Lekadir, K., Camara, O., Gonzalez Ballester, M.A., Sanroma, G., Napel, S., Petersen, S., Tziritas, G., Griniias, E., Khened, M., Kollerathu, V.A., Krishnamurthi, G., Rohé, M.M., Pennec, X., Sermesant, M., Isensee, F., Jäger, P., Maier-Hein, K.H., Full, P.M., Wolf, I., Engelhardt, S., Baumgartner, C.F., Koch, L.M., Wolterink, J.M., Igum, I., Jang, Y., Hong, Y., Patravali, J., Jain, S., Humbert, O., Jodoin, P.M., 2018. Deep learning techniques for automatic mri cardiac multi-structures segmentation and diagnosis: Is the problem solved? *IEEE Transactions on Medical Imaging* 37, 2514–2525.
- Can, Y.B., Chaitanya, K., Mustafa, B., Koch, L.M., Konukoglu, E., Baumgartner, C.F., 2018. Learning to segment medical images with scribble-supervision alone. *Deep Learning in Medical Image Analysis and Multimodal Learning for Clinical Decision Support Workshop*.
- Chaitanya, K., Karani, N., Baumgartner, C.F., Becker, A., Donati, O., Konukoglu, E., 2019. Semi-supervised and task-driven data augmentation. *International Conference on Information Processing in Medical Imaging*, 29–41.
- Chen, J., Huang, W., Zhang, J., Debattista, K., Han, J., 2025a. Addressing inconsistent labeling with cross image matching for scribble-based medical image segmentation. *IEEE Transactions on Image Processing* 34, 842–853.
- Chen, Q., Lyu, H., Hu, X., Lu, Y., Hong, Y., 2025b. Volumetric medical image segmentation via scribble annotations and shape priors. *Machine Vision and Applications* 36, 22.
- Du Plessis, M., Niu, G., Sugiyama, M., 2015. Convex formulation for learning from positive and unlabeled data. *International Conference on Machine Learning*, 1386–1394.
- Fong, R., Patrick, M., Vedaldi, A., 2019. Understanding deep networks via extremal perturbations and smooth masks, pp. 2950–2958.
- Fong Ruth, Patrick M, V.A., 2017. Interpretable explanations of black boxes by meaningful perturbation, pp. 3429–343.
- Gao, F., Hu, M., Zhong, M.E., Feng, S., Tian, X., Meng, X., Huang, Z., Lv, M., Song, T., Zhang, X., et al., 2022. Segmentation only uses sparse annotations: Unified weakly and semi-supervised learning in medical images. *Medical Image Analysis* 80, 102515.
- Gao, S., Zhuang, X., 2020. Robust approximations of low-rank minimization for tensor completion. *Neurocomputing* 379, 319–333.
- Garcea, F., Serra, A., Lamberti, F., Morra, L., 2023. Data augmentation for medical imaging: A systematic literature review. *Computers in biology and medicine* 152, 106391.
- Garg, S., Wu, Y., Smola, A.J., Balakrishnan, S., Lipton, Z., 2021. Mixture proportion estimation and pu learning: A modern approach. *Advances in Neural Information Processing Systems* 34.
- Han, M., Luo, X., Xie, X., Liao, W., Zhang, S., Song, T., Wang, G., Zhang, S., 2024. Dmsps: Dynamically mixed soft pseudo-label supervision for scribble-supervised medical image segmentation. *Medical Image Analysis* 97, 103274.
- Isensee, F., Jaeger, P.F., Kohl, S.A., Petersen, J., Maier-Hein, K.H., 2021. nnu-net: a self-configuring method for deep learning-based biomedical image segmentation. *Nature Methods* 18, 203–211.
- Ji, Z., Shen, Y., Ma, C., Gao, M., 2019. Scribble-based hierarchical weakly supervised learning for brain tumor segmentation. *International Conference on Medical Image Computing and Computer-Assisted Intervention*, 175–183.
- Jia, Z., Huang, X., Chang, E.I.C., Xu, Y., 2017. Constrained deep weak supervision for histopathology image segmentation. *IEEE transactions on medical imaging* 36, 2376–2388.
- Kervadec, H., Dolz, J., Tang, M., Granger, E., Boykov, Y., Ayed, I.B., 2019. Constrained-cnn losses for weakly supervised segmentation. *Medical Image Analysis* 54, 88–99.
- Khoreva, A., Benenson, R., Hosang, J., Hein, M., Schiele, B., 2017. Simple does it: Weakly supervised instance and semantic segmentation. *IEEE Conference on Computer Vision and Pattern Recognition*, 876–885.
- Kim, J., Choo, W., Jeong, H., Song, H.O., 2021. Co-mixup: Saliency guided joint mixup with supermodular diversity. *International Conference on Learning Representations*.
- Kim, J.H., Choo, W., Song, H.O., 2020. Puzzle mix: Exploiting saliency and local statistics for optimal mixup. *International conference on machine learning*, 5275–5285.
- Kiryo, R., Niu, G., du Plessis, M.C., Sugiyama, M., 2017. Positive-unlabeled learning with non-negative risk estimator. *Advances in Neural Information Processing Systems* 30.
- Kohl, S., Romera-Paredes, B., Meyer, C., De Fauw, J., Ledsam, J.R., Maier-Hein, K., Eslami, S., Jimenez Rezende, D., Ronneberger, O., 2018. A probabilistic u-net for segmentation of ambiguous images. *Advances in neural information processing systems* 31.
- Kuang, Z., Yan, Z., Zhou, H., Yu, L., 2023. Cluster-re-supervision: Bridging the gap between image-level and pixel-wise labels for weakly supervised medical image segmentation. *IEEE Journal of Biomedical and Health Informatics* 27, 4890–4901.
- Kweon, H., Yoon, S.H., Yoon, K.J., 2023. Weakly supervised semantic segmentation via adversarial learning of classifier and reconstructor. *IEEE Conference on Computer Vision and Pattern Recognition*, 11329–11339.
- Landman, B., Xu, Z., Igelsias, J., Styner, M., Langerak, T., Klein, A., 2015. Miccai multi-atlas labeling beyond the cranial vault—workshop and challenge. *Proc. MICCAI Multi-Atlas Labeling Beyond Cranial Vault Workshop Challenge* 5, 12.
- Latince, P., Saerens, M., Decaestecker, C., 2001. Adjusting the outputs of a classifier to new a priori probabilities may significantly improve classification accuracy: evidence from a multi-class problem in remote sensing. *International Conference on Machine Learning* 1, 298–305.
- Li, L., Wu, F., Wang, S., Luo, X., Martin-Isala, C., Zhai, S., Zhang, J., Liu, Y., Zhang, Z., Ankenbrand, M.J., et al., 2022. Myops: A benchmark of myocardial pathology segmentation combining three-sequence cardiac magnetic resonance images. *arXiv preprint arXiv:2201.03186*.
- Li, Z., Zheng, Y., Shan, D., Yang, S., Li, Q., Wang, B., Zhang, Y., Hong, Q., Shen, D., 2024. Scribformer: Transformer makes cnn work better for scribble-based medical image segmentation. *IEEE Transactions on Medical Imaging* 43, 2254–2265.
- Lin, L., Liu, Y., Wu, J., Cheng, P., Cai, Z., Wong, K.K., Tang, X., 2024. Fedlppa: Learning personalized prompt and aggregation for federated weakly-supervised medical image segmentation. *IEEE Transactions on Medical Imaging*, 1127–1139.
- Lin, Y., Qu, Z., Chen, H., Gao, Z., Li, Y., Xia, L., Ma, K., Zheng, Y., Cheng, K.T., 2023. Nuclei segmentation with point annotations from pathology images via self-supervised learning and co-training. *Medical Image Analysis* 89, 102933.
- Liu, J., Tan, S.Y., Yang, X., Xu, Y., Yeo, S.Y., 2025a. Effdnet: A scribble-supervised medical image segmentation method with enhanced foreground feature discrimination. *International Conference on Medical Image Computing and Computer-Assisted Intervention*, 194–204.
- Liu, X., Yuan, Q., Gao, Y., He, K., Wang, S., Tang, X., Tang, J., Shen, D., 2022. Weakly supervised segmentation of covid19 infection with scribble annotation on ct images. *Pattern Recognition* 122, 108341.
- Liu, X., Zhang, J., Zhang, Y., Chen, L., Luo, L., Tang, J., 2025b. Weakly supervised segmentation of retinal layers on oct images with amd using uncertainty prototype and boundary regression. *Medical Image Analysis* 102, 103572.
- Luo, X., Hu, M., Liao, W., Zhai, S., Song, T., Wang, G., Zhang, S., 2022. Scribble-supervised medical image segmentation via dual-branch network and dynamically mixed pseudo labels supervision. *International Conference on Medical Image Computing and Computer-Assisted Intervention*, 528–538.
- McLachlan, G.J., Krishnan, T., 2007. *The EM algorithm and extensions*. John Wiley & Sons.
- Meng, Z., Zhe, X., Kang, Z., Raymond, K.y.T., 2023. Weakly supervised med-

- ical image segmentation via superpixel-guided scribble walking and class-wise contrastive regularization. *International Conference on Medical Image Computing and Computer-Assisted Intervention*, 137–147.
- Obukhov, A., Georgoulis, S., Dai, D., Gool, L.V., 2019a. Gated cxf loss for weakly supervised semantic image segmentation. *arXiv preprint arXiv:1906.04651*.
- Obukhov, A., Georgoulis, S., Dai, D., Van Gool, L., 2019b. Gated cxf loss for weakly supervised semantic image segmentation. *arXiv preprint arXiv:1906.04651*.
- Ouali, Y., Hudelot, C., Tami, M., 2020. Semi-supervised semantic segmentation with cross-consistency training. *IEEE Conference on Computer Vision and Pattern Recognition*, 12674–12684.
- Qin, H., Jin, X., Zhu, H., Liao, H., El-Yacoubi, M.A., Gao, X., 2024. Sumix: Mixup with semantic and uncertain information. *European Conference on Computer Vision*, 70–88.
- Rajchl, M., Koch, L.M., Ledig, C., Passerat-Palmbach, J., Misawa, K., Mori, K., Rueckert, D., 2017. Employing weak annotations for medical image analysis problems. *arXiv preprint arXiv:1708.06297*.
- Ramaswamy, H., Scott, C., Tewari, A., 2016. Mixture proportion estimation via kernel embeddings of distributions. *International Conference on Machine Learning*, 2052–2060.
- Roth, H.R., Yang, D., Xu, Z., Wang, X., Xu, D., 2021. Going to extremes: weakly supervised medical image segmentation. *Machine Learning and Knowledge Extraction* 3, 507–524.
- Sakai, T., Plessis, M.C., Niu, G., Sugiyama, M., 2017. Semi-supervised classification based on classification from positive and unlabeled data. *International Conference on Machine Learning*, 2998–3006.
- Tajbakhsh, N., Jeyaseelan, L., Li, Q., Chiang, J.N., Wu, Z., Ding, X., 2020. Embracing imperfect datasets: A review of deep learning solutions for medical image segmentation. *Medical Image Analysis* 63, 101693.
- Tang, M., Perazzi, F., Djelouah, A., Ben Ayed, I., Schroers, C., Boykov, Y., 2018. On regularized losses for weakly-supervised cnn segmentation. *European Conference on Computer Vision*, 507–522.
- Tarvainen, A., Valpola, H., 2017. Mean teachers are better role models: Weight-averaged consistency targets improve semi-supervised deep learning results. *Advances in Neural Information Processing Systems* 30.
- Valvano, G., Leo, A., Tsaftaris, S.A., 2021. Learning to segment from scribbles using multi-scale adversarial attention gates. *IEEE Transactions on Medical Imaging* 40, 1990–2001.
- Wang, D., Zhang, Y., Zhang, K., Wang, L., 2020. Focalmix: Semi-supervised learning for 3d medical image detection. *IEEE Conference on Computer Vision and Pattern Recognition*, 3951–3960.
- Wang, W., Sun, G., Van Gool, L., 2022. Looking beyond single images for weakly supervised semantic segmentation learning. *IEEE Transactions on Pattern Analysis and Machine Intelligence* 46, 1635–1649.
- Wei, J., Hu, Y., Cui, S., Zhou, S.K., Li, Z., 2023. Weakpolyp: You only look bounding box for polyp segmentation. *International Conference on Medical Image Computing and Computer-Assisted Intervention*, 757–766.
- Wu, F., Zhuang, X., 2022. Minimizing estimated risks on unlabeled data: A new formulation for semi-supervised medical image segmentation. *IEEE Transactions on Pattern Analysis and Machine Intelligence* 45, 6021–6036.
- Yang, J., Mehta, N., Demirci, G., Hu, X., Ramakrishnan, M.S., Naguib, M., Chen, C., Tsai, C.L., 2024. Anomaly-guided weakly supervised lesion segmentation on retinal oct images. *Medical image analysis* 94, 103139.
- Yue, Q., Luo, X., Ye, Q., Xu, L., Zhuang, X., 2019. Cardiac segmentation from lge mri using deep neural network incorporating shape and spatial priors. *International Conference on Medical Image Computing and Computer-Assisted Intervention*, 559–567.
- Yun, S., Han, D., Oh, S.J., Chun, S., Choe, J., Yoo, Y., 2019. Cutmix: Regularization strategy to train strong classifiers with localizable features. *International Conference on Computer Vision*, 6023–6032.
- Zhang, B., Xiao, J., Jiao, J., Wei, Y., Zhao, Y., 2021. Affinity attention graph neural network for weakly supervised semantic segmentation. *IEEE Transactions on Pattern Analysis and Machine Intelligence* 44, 8082–8096.
- Zhang, H., Cisse, M., Dauphin, Y.N., Lopez-Paz, D., 2018. mixup: Beyond empirical risk minimization. *International Conference on Learning Representations*.
- Zhang, K., Zhuang, X., 2022a. Cyclemix: A holistic strategy for medical image segmentation from scribble supervision. *IEEE Conference on Computer Vision and Pattern Recognition*, 11656–11665.
- Zhang, K., Zhuang, X., 2022b. Shapepu: A new pu learning framework regularized by global consistency for scribble supervised cardiac segmentation. *Medical Image Computing and Computer Assisted Intervention*, 162–172.
- Zhang, P., Zhong, Y., Li, X., 2020. AccI: Adversarial constrained-cnn loss for weakly supervised medical image segmentation. *arXiv preprint arXiv:2005.00328*.
- Zhang, X., Wu, S., Zhang, P., Jin, Z., Xiong, X., Bu, Q., Chen, J., Feng, J., 2025. Helpnet: Hierarchical perturbations consistency and entropy-guided ensemble for scribble supervised medical image segmentation. *Medical Image Analysis* 105, 103719.
- Zhao, X., Wang, L., Zhang, Y., Han, X., Deveci, M., Parmar, M., 2024. A review of convolutional neural networks in computer vision. *Artificial Intelligence Review* 57, 99.
- Zhou, B., Khosla, A., Lapedriza, A., Oliva, A., Torralba, A., 2016. Learning deep features for discriminative localization. *IEEE Conference on Computer Vision and Pattern Recognition*, 2921–2929.
- Zhu, J.Y., Park, T., Isola, P., Efros, A.A., 2017. Unpaired image-to-image translation using cycle-consistent adversarial networks. *IEEE International Conference on Computer Vision*, 2223–2232.
- Zhuang, X., 2016. Multivariate mixture model for cardiac segmentation from multi-sequence mri. *Medical Image Computing and Computer Assisted Intervention*, 2933–2946.
- Zhuang, X., 2019a. Multivariate mixture model for myocardial segmentation combining multi-source images. *IEEE transactions on pattern analysis and machine intelligence* 41, 2933–2946.
- Zhuang, X., 2019b. Multivariate mixture model for myocardial segmentation combining multi-source images. *IEEE Transactions on Pattern Analysis and Machine Intelligence* 41, 2933–2946.
- Zou, D., Cao, Y., Li, Y., Gu, Q., 2023. The benefits of mixup for feature learning. *International Conference on Machine Learning*, 43423–43479.